Static voltage stability analysis based on continuation power flow

by

Zhongjun Yu

A Thesis Submitted to the

Graduate Faculty in Partial Fulfillment of the

Requirements for the Degree of

MASTER OF SCIENCE

Department: Electrical Engineering and Computer Engineering

Major: Electrical Engineering

Iowa State University

Ames, Iowa

1993

TABLE OF CONTENTS

LIST OF TABLES

LIST OF FIGURES

ACKNOWLEDGMENTS

I would like to thank my advisor Dr. V. Ajjarapu for introducing me to the research area, for offering intellectual advice, and for providing financial support. I would also like to thank Dr. J. Lamont and Dr. R. Gregorac for reviewing my thesis and for giving me useful suggestions. Special thanks go to Dr. A. A. Fouad for his kindness and encouragement when I first came to Iowa State University. Finally, I would like to thank Dr. V. Vittal for serving as my temporary advisor and for his advice.

CHAPTER 1. INTRODUCTION

1.1 Background on the Voltage Stability Problem

Voltage stability is a major challenge facing many utilities today. Although voltage control problems have always been important and have been a major concern in developing networks, the problems in more mature networks have arisen fairly recently [1]. They result in large part to intensive use of available transmission between load centers and remotely sited generation. Furthermore, the problems are made worse by the continued growth in society's electric energy demand and the relative slowness of constructing new power plants or transmitting lines leading to systems working closer and closer to their capacity limits.

In a heavily loaded power system, if the injected reactive power is insufficient the voltage stability is very vulnerable. In some highly interconnected systems, when there is a generator loss, a transmission line loss or a large unforeseen load increase, the voltage may drop quickly and the manual or automatic system control may not be able to halt the drop [2]. Then the voltage drop continues leading to complete blackout of a large area. This phenomenon is called voltage collapse. There have been many voltage collapse incidents around the world in recent years with increased frequency in recent years, resulting in enormous economic loss.

1.2 Scope and Objective

In response to utilities' increasing concern over voltage stability, many researchers have been trying to understand the mechanisms of voltage collapse in order to prevent it. Many papers have been published on voltage collapse, and various methods have been proposed to predict and to prevent it. Basically, these methods use two approaches: static and dynamic. One well accepted theory [2] explains the voltage collapse as a consequence of the loss of a stable equilibrium point through a saddle node bifurcation when the total system active power load is increased to a critical level. At this critical load, the Jacobian of the power flow equation becomes singular. Therefore, a key in studying voltage collapse is to find the Jacobian singularity, which is equivalent to finding the critical load. The continuation power flow method [3] developed at Iowa State University was designed to accomplish these tasks.

The objective of this research is to improve the continuation power flow (CPF) method by incorporating several new techniques, thus making the CPF method capable of

- finding the critical point in the minimum number of steps by using an optimal step length selection based on reactive power generation sensitivity, with improved accuracy;
- providing useful information on system voltage security for a given load change scenario by calculating margins to voltage instability and by revealing weak buses in the system;
- identifying the worst case load change scenario and finding the worst case margin to voltage collapse;
- providing the optimal strategy for load shedding to regain voltage stability when the initial load is in the unsolvable region.

1.3 Thesis Outline

Chapter 2 describes the basic principles of the continuation power flow method. In Chapter 3, we first derive the formula for calculating the sensitivity of reactive power generation to load increases and then present the optimal strategy for selecting step length for the CPF. This optimal step length is the maximum length that can be used in each step without any generator exceeding its reactive generation limit. Chapter 4 presents the important issue of voltage stability margin. We review two measures for proximity to voltage instability and present the margin to voltage instability in terms of MW (active load) distance and MVAr (reactive power reserve) distance to voltage collapse. In Chapter 5 we incorporate a recent research result on normal vector of the critical boundary into the CPF and present an iterative procedure for calculating the worst case load change scenario, and the worst case margin to voltage collapse. Chapter 6 studies the problem of optimal load shedding, which uses the minimal amount of load shedding along the most effective direction to move an unsolvable load into the solvable region. Finally Chapter 7 concludes the thesis with some remarks on related research issues.

CHAPTER 2. CONTINUATION POWER FLOW

2.1 Introduction

The continuation power flow method was developed at Iowa State University [3] by applying the well-known mathematical continuation algorithm to the solution of the static power flow equations. The purpose of the continuation power flow method is to find a continuum of power flow solutions for a given load change scenario and to find the critical point. The basic principle of the continuation power flow is rather simple. It employs a predictor-corrector scheme to trace a solution path of the power flow equation parameterized by a load change parameter. As illustrated in Figure 2.1, it starts from a known solution and predicts a subsequent solution along the tangent direction for a different value of the load parameter. This predictor is then corrected by using the well-known Newton-Raphson technique for the power flow equation. This process is repeated until the critical point is reached, where the component of the tangent vector corresponding to load parameter becomes zero.

In the next section, we reformulate the static load flow equation to include a load change direction and a load change parameter. Then, the formula for predicting the next solution will be presented, together with the correcting process. Finally, we will discuss some important issues concerning the continuation power flow method.

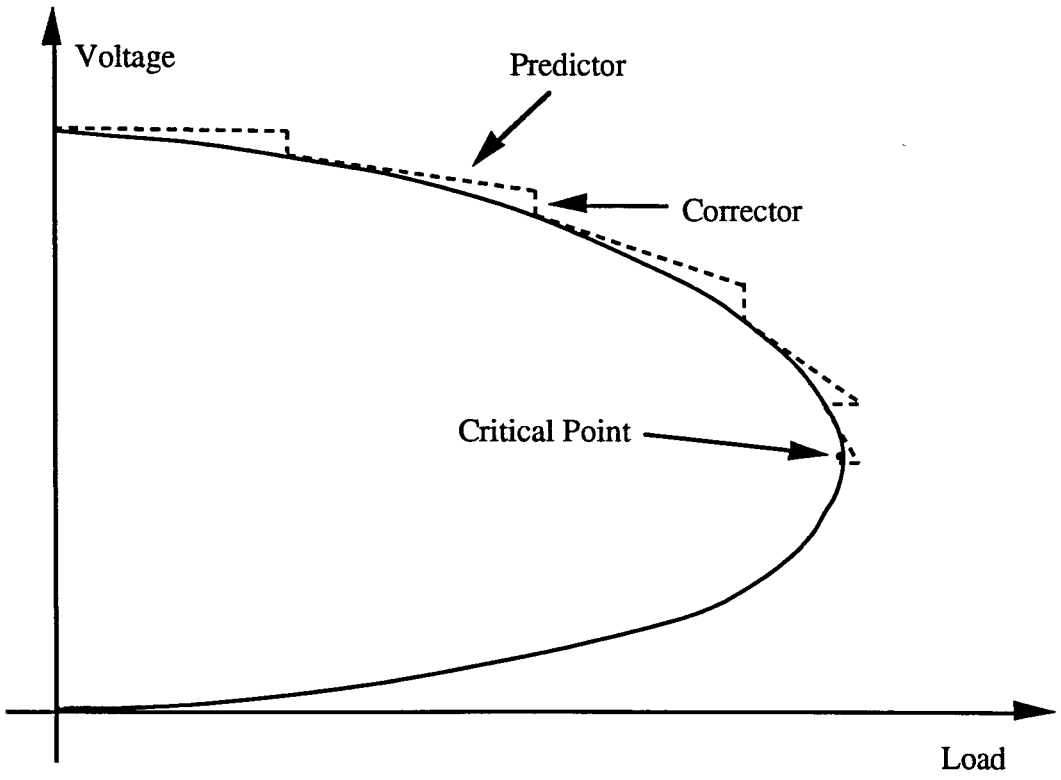

Figure 2.1: An illustration of the predictor-corrector scheme used in the continuation power flow

2.2 Parameterized Static Power Flow Equation

The static power flow equation represents the power balance at each bus. Therefore, for each bus i of an n bus system, we have:

$$\Delta P_i = P_{Gi} - P_{Li} - P_{Ti} = 0 \tag{2.1}$$

$$\Delta Q_i = Q_{Gi} - Q_{Li} - Q_{Ti} = 0 \tag{2.2}$$

where P stands for the real power, Q stands for reactive power, and the subscripts L, G, T denote bus load, generation and injection respectively. Let $V_i \angle \delta_i$ be the voltage and

angle at bus i, and let $y_{ij}\angle v_{ij}$ be the $(i,j)th$ element of the bus admittance matrix Y_{bus}. The real and reactive injections at bus i are of the form:

$$P_{Ti} = \sum_{j=1}^{n} V_i V_j y_{ij} \cos(\delta_i - \delta_j - v_{ij}) \tag{2.3}$$

$$Q_{Ti} = \sum_{j=1}^{n} V_i V_j y_{ij} \sin(\delta_i - \delta_j - v_{ij}) \tag{2.4}$$

To simulate a load change, P_{Li} and Q_{Li} are parameterized by a load change parameter λ in the following form:

$$P_{Li} = P_{Li0} + \lambda(K_{Li} S_{\Delta BASE} \cos\varphi_i) \tag{2.5}$$

$$Q_{Li} = Q_{Li0} + \lambda(K_{Li} S_{\Delta BASE} \sin\varphi_i) \tag{2.6}$$

where

P_{Li0} : initial real load at bus i

Q_{Li0} : initial reactive load at bus i

K_{Li} : multiplier designating the rate of load change at bus i as λ changes

φ_i : power factor angle of load change at bus i

$S_{\Delta BASE}$: a given quantity of apparent power which is chosen to provide appropriate scaling of λ

In addition, the active power generation term can be expressed in terms of λ as:

$$P_{Gi} = P_{Gi0}(1 + \lambda K_{Gi}) \tag{2.7}$$

where P_{Gi0} is the initial active generation at bus and K_{Gi} is a constant used to specify the rate of change in generation at bus i as λ varies.

Then the parameterized power flow equations become:

$$0 = P_{Gi0}(1 + \lambda K_{Gi}) - P_{Li0} - \lambda(K_{Li} S_{\Delta BASE} \cos\varphi_i) - P_{Ti} \tag{2.8}$$

$$0 = Q_{Gi0} - Q_{Li0} - \lambda(K_{Li} S_{\Delta BASE} \sin\varphi_i) - Q_{Ti} \tag{2.9}$$

Let V and δ be the vector of bus voltage angle. Then, the power flow equation can be written in a more compact form:

$$F(\delta,V,\lambda)=0 \qquad (2.10)$$
$$0\le\lambda\le\lambda_{critical}$$

For each λ, the above equation admits some solutions. As λ varies, $\delta(\lambda)$, $V(\lambda)$ form branches of the solution curves. When λ reaches the critical value, two branches meet and the Jacobian matrix of F with respect to δ and V becomes singular, and the system loses voltage stability. The continuation power flow method starts at a known solution and traces one branch to find the critical point.

2.3 Prediction and Correction

Once a base solution for $\lambda=0$ has been found, a prediction of the next solution can be made along the tangent direction of the solution path. To do this, we differentiate the equation (2.10) to get

$$dF(\delta,V,\lambda)=F_\delta d\delta+F_V dV+F_\lambda d\lambda=0$$

or

$$\begin{bmatrix}F_\delta & F_V & F_\lambda\end{bmatrix}\begin{bmatrix}d\delta\\ dV\\ d\lambda\end{bmatrix}=0 \qquad (2.11)$$

Because of the inclusion of the load change parameter λ, the above equation contains one more unknown than the number of equations. To ensure the unique solution, one more constraint needs to be introduced. In the continuation power flow method, we simply require that the *kth* component of the tangent vector should be unity [4], i.e., let

$$t = \begin{bmatrix} d\delta \\ dV \\ d\lambda \end{bmatrix}, \quad t_k = \pm 1$$

The selection of the index k and the sign of t_k will be discussed later. With this added constraint, we have

$$\begin{bmatrix} F_\delta & F_V & F\lambda \\ & e_k & \end{bmatrix} \cdot t = \begin{bmatrix} 0 \\ \pm 1 \end{bmatrix} \tag{2.12}$$

where e_k is a row vector with all zero elements except the *kth* element, which is 1.

Once the tangent vector t is found by solving the above equation, the prediction for the next solution can be made as follows:

$$\begin{bmatrix} \delta^* \\ V^* \\ \lambda^* \end{bmatrix} = \begin{bmatrix} \delta \\ V \\ \lambda \end{bmatrix} + \sigma \begin{bmatrix} d\delta \\ dV \\ d\lambda \end{bmatrix} \tag{2.13}$$

where the superscript * denotes prediction, and σ is a scalar representing the step length. The selection of the step length will be addressed in detail later.

Now that a prediction has been made, a method of correcting the approximate solution is needed. This is necessary because $\begin{bmatrix} \delta^* \\ V^* \\ \lambda^* \end{bmatrix}$ is a point along the tangent vector direction, but is not the actual solution to the power flow equations. However, as long as the step length is not too large, this prediction is near, but not on the solution curve, and the Newton-Raphson method can be used to find the point on the curve that is closest to the prediction. However, before we can do this, a small problem needs to be solved. Because of inclusion of the load parameter λ, equation (2.10) contains one more unknown than the number of the equations. This can easily be handled by letting one of

the solution components be fixed, thus introducing one more equation. Mathematically, this is done as follows:

let $$x = \begin{bmatrix} \delta \\ V \\ \lambda \end{bmatrix}$$

and introduce $$x_k = \eta$$

where η is the appropriate value for the *kth* element of x. Then the power flow equation becomes:

$$\begin{bmatrix} F(x) \\ x_k - \eta \end{bmatrix} = 0 \tag{2.14}$$

This index k above can be, in theory, any integer between 1 and $m+1$, where m is the dimension of x. However, in the continuation power flow method, we use the same index k as in the prediction. The corresponding state variable x_k is called the continuation parameter.

To select the continuation parameter, we use the following rule, which, in our experience, works quite nicely. In each step we select the state variable with the largest corresponding tangent vector component as the continuation parameter. For the first step we will choose λ to be the continuation parameter. Therefore:

$$x_k = \begin{cases} \lambda, & \textit{first step} \\ x_k : |t_k| = \max\{|t_1|, |t_2|, \cdots |t_m|\}, & \textit{else} \end{cases}$$

Here, t is the tangent vector and m is the dimension of x. Note that in the first few steps $d\lambda$ is generally the largest, hence λ is used as the continuation parameter. However, as the critical point is approached, $d\lambda$ may not be as large as some of the $|dV_i|$'s. Therefore a bus voltage is used as the continuation parameter.

2.4 Load Change Direction

In the formulation of Section 2.2, if we let

$$C_{Pi} = K_{Li} S_{\Delta BASE} \cos\varphi_i$$

$$C_{Qi} = K_{Li} S_{\Delta BASE} \sin\varphi_i$$

and

$$C_P = \begin{bmatrix} C_{P1} \\ C_{P2} \\ \vdots \\ C_{Pn} \end{bmatrix}, \quad C_Q = \begin{bmatrix} C_{Q1} \\ C_{Q2} \\ \vdots \\ C_{Qn} \end{bmatrix}$$

Then the load change can be simply modeled as:

$$P_L = P_{L0} + \lambda C_P$$

$$Q_L = Q_{L0} + \lambda C_Q$$

where $P_{L0} = \begin{bmatrix} P_{L01} & P_{L02} & \cdots & P_{L0n} \end{bmatrix}^T$ is the vector of the initial real load, Q_{L0} is the vector of the initial reactive load, P_L is the increased real load and Q_L is the increased reactive load. As λ varies, $\begin{bmatrix} P_L \\ Q_L \end{bmatrix}$ lies on a straight line starting at $\begin{bmatrix} P_{L0} \\ Q_{L0} \end{bmatrix}$, and moves in the direction of $\begin{bmatrix} C_P \\ C_Q \end{bmatrix}$. Therefore $C = \begin{bmatrix} C_P \\ C_Q \end{bmatrix}$ is called the load change direction.

Once the load change direction is given, the variation in the load change parameter λ defines a solution path leading to a critical point. When $\min\left|\frac{Cd\lambda}{dV_i}\right| \to 0$, a very small load increase can cause a large voltage drop; therefore, the critical point can be identified by $\min\left|\frac{Cd\lambda}{dV_i}\right| = 0$. If C is changed, we will have a different critical point. If C is allowed to vary gradually, the corresponding critical points form a hyper surface in the voltage angle

and voltage magnitude space. We call this surface the critical surface. Inside the surface, the system is stable; outside, the system is not stable.

For a given power system and a given load increase direction, the performance of the continuation power flow method in finding the critical point depends largely on the proper selection of the step length. In the next chapter we present a strategy for selecting an optimal step length based on reactive power generation sensitivity. This strategy provides the minimum number of steps for reaching the critical point.

CHAPTER 3. SENSITIVITY-BASED OPTIMAL STEP LENGTH

3.1 Introduction

In the last chapter, we reviewed the basic principles of the continuation power flow method, which forms the basis of our research. As mentioned there, the selection of step length is a very important part of the continuation power flow algorithm, since computational speed and convergence performance are both greatly affected by the choice of the step length. For an example, if we use a fixed step length that is too small, then we have to perform a very large number of prediction and correction iterations before we reach the critical point. Therefore, the computation is going to be very time consuming. Furthermore, this large number of computations will inevitably introduce more numerical errors because of round-off accumulation. On the other hand, if we use a fixed step length that is too large, then the predictor may be very far from the solution curve. That means the initial guess for the subsequent Newton-Raphson iterations in the correction process may be very far from the final desired value. Therefore, the N-R iteration may lead to divergence.

In this chapter, we incorporate some recent results of Flatabø, *et al.*. [5] on the use of sensitivity technique and apply them to the continuation power flow method to develop a sensitivity-based strategy for selecting the optimal step length. To do this, we will

first develop the formula for calculating the sensitivity of reactive power generation to system active load changes. Then in Section 3.3, we present the procedure for optimal step length selection for the continuation power flow. Finally, test results based on the optimal step length strategy can be presented.

3.2 Sensitivity of Reactive Power Generation

The reactive power at a generator bus can be defined as the function Q_i in the following way [6]:

$$Q_i = Q_{Li0} + \lambda(K_{Li} S_{\Delta BASE} \sin(\varphi_i)) + Q_{Ti} \tag{3.1}$$

where

$$Q_{Ti} = \sum_{j=1}^{n} V_i V_j \sin(\delta_i - \delta_j - \theta_{ij})$$

is the reactive power injection at bus i and

λ = load change parameter

Q_{Li0} = initial reactive load

K_{Li} = a multiplier to designate the rate of load change at bus i as λ changes

φ_i = the power factor angle of load change at bus i

$S_{\Delta BASE}$ = the apparent power that is chosen to provide appropriate scaling of λ

Therefore, the sensitivity of a reactive power generation to the variations of load parameter λ [6] is given by

$$\frac{dQ_i}{d\lambda} = \sum_{j=1}^{n} \frac{\partial Q_{Ti}}{\partial x_j} \cdot \frac{dx_j}{d\lambda} + K_{Li} S_{\Delta BASE} \sin(\varphi_i)$$

where x is the state variable and $\frac{dx_j}{d\lambda}$ can be directly obtained from the components of the tangent vector in the continuation power flow.

3.3 Optimal Step Length Selection

The calculation of the critical point of voltage collapse is carried out in steps. At each step, we need to choose an optimal step length so that the critical point can be obtained accurately without causing any numerical trouble. Previously, the step length was selected on the basis of the curvature at the solution point of the previous step [7]. In such an approach, the corresponding reactive power generation Q's in the next solution may exceed their limits or may be smaller than their limits.

The basic idea of the optimal step length selection is as follows. In each step, we select the step length such that after the load is increased, at least one generator reaches its MVAr generation limit and all the other generators are still within their MVAr generation limits. This is the maximum step length that can be used, since any larger step length leads to at least one generator exceeding its reactive power generation limit.

This optimal step length is calculated by using the sensitivity technique as follows:

In each step n, we first calculate a candidate step length $\Delta\lambda_j^{(n)}$ for each generator as follows:

$$\Delta\lambda_j^{(n)} = \frac{Q_{j\max} - Q_j}{dQ_j/d\lambda}$$

From equation (3.1), we know that $Q_j(x,\lambda)$ has a linear relation to λ; thus if we choose $\Delta\lambda_j^{(n)}$ as above, we can guarantee that the MVAr-generation of generator j reaches its reactive power limit. Then we set

$$\Delta\lambda^{(n)} = \min_j \Delta\lambda_j^{(n)}$$

where

$\Delta\lambda^{(n)}$ = the maximum value that λ can be increased

$Q_{j\max}$ = maximum MVAr-generating capacity of plant j

j = the bus number corresponding to the generators

Therefore, if λ is increased by $\Delta\lambda^{(n)}$, then at least one generator will reach its reactive power generation limit, but no generator will exceed its limit.

The step length at step n is finally selected to be

$$\sigma^{(n)} = \Delta\lambda^{(n)} / d\lambda$$

where $d\lambda$ can be directly given by tangent vector. Note that if the generator at bus j reaches its maximum MVAr capacity at any particular step n, then bus j has to be changed to PQ bus.

3.4 Simulation Results

The optimal step length described in the last section has been incorporated into the continuation power flow method. Its performance has been tested by using the Iowa reduced system and the New England 30-bus system, whose single line diagram is given in Figure 3.1. There are a total of 9 generators and 20 PQ buses in the system. Tables 3.1 and 3.2 list the number of steps and the total number of Newton-Raphson iterations. For comparison, we also applied the curvature-based step length method [7] to the same system, with the same base case and same load change direction. The number of steps and the total number of N-R iterations are also listed in the same table. It can be seen that by using the optimal step length, the number of steps is greatly reduced. This is expected, since the optimal step length is the maximum step length. But the total load change before the critical point is independent of methods and therefore is the same for both cases. Hence

the larger step length leads to the smaller number of steps. However, the total number of N-R iterations is reduced only by a small percentage. The reason may be that the initial guess for Newton-Raphson iteration in the correction process is further away from the solution curve because of the larger prediction steps.

With a proper step length strategy, the continuation power flow method can find the critical power flow easily. The next chapter studies another important issue in static voltage stability analysis: margins to voltage instability.

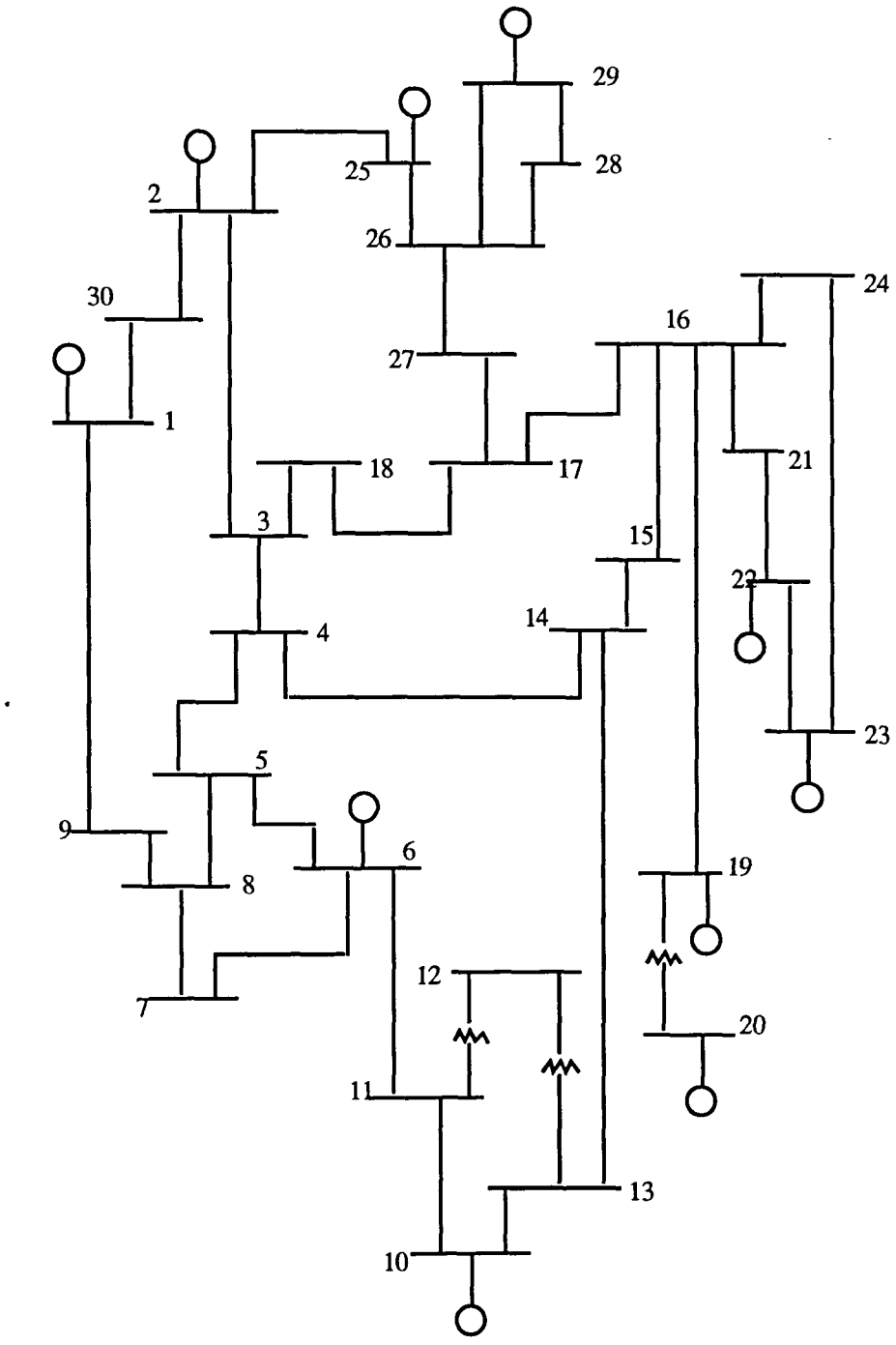

Figure 3.1: The New England 30-bus system [8]

Table 3.1: Performance of optimal step length method (30-bus system)

	# of steps	# of N-R iterations	Critical load
Optimal step length	7	77	9579 MW
Curvature-based step length	12	80	9570 MW

Table 3.2: Performance of optimal step length method (162-bus system)

	# of steps	# of N-R iterations	Critical load
Optimal step length	8	48	3209 MW
Curvature-based step length	12	49	3213 MW

CHAPTER 4. MARGINS TO VOLTAGE INSTABILITY

4.1 Introduction

In the previous chapter, we defined the critical point. It can be calculated by using the continuation power flow method with small step lengths. But small step lengths may require a great deal of computation. To reduce computation, we can use larger step lengths and then estimate the critical point by the method [9-10] discussed in Appendix A. The next problem of extreme importance in studying power system security and in preventing voltage collapse is to determine how far away the current operating point is from the critical point. The purpose to calculate voltage stability margins is to quantify the distance from a particular operating point to the point of steady-stable voltage collapse. The information so obtained could then be used for setting of transfer limits in the network during power system planning studies.

In the recent literature, Several methods designed for a similar purpose have been described. The voltage stability index proposed by Ajjarapu and Christy [11] uses the negative inverse of the sensitivity of bus voltage magnitude to the system load as a proximity measure to voltage collapse. This index is positive when the operating point is stable, approaches zero when the critical point is approached, and becomes negative when the system load exceeds the critical value. Different voltage stability indices are also defined by using the smallest singular value of the Jacobian matrix [12-13] or using the smallest real

part of the eigenvalues of the Jacobian [14]. All these indices have similar advantages and disadvantages. The margins for voltage instability, on the other hand, offer some improvements in performance through calculating the MW-distance or reactive power reserve to voltage instability.

For the purpose of comparison, we will first review the different voltage stability indices in the next two sections together with some application examples. Then we will present in Section 4.4 the theory and procedure for calculating margins to voltage instability as used in the continuation power flow method. Simulation results for the New England 30-bus test system and the 162-bus Iowa reduced system will be presented in Section 4.5. These results will be compared to the performance of voltage stability indices.

4.2 Voltage Stability Index

The voltage stability index defined by Ajjarapu and Christy [11] has the dual capability of identifying weak buses and measuring the proximity to voltage collapse. This index, which is designed for the continuation power flow method, uses the sensitivity information available from the tangent vector of the continuation predictor. Thus, the calculation is quite inexpensive.

In the continuation power flow method, the tangent vector describes the direction of the solution path at a corrected solution point. Since the elements of the tangent vector represent differential changes in the state variables (dV_i or $d\delta_i$) in response to a differential change in the load parameter ($d\lambda$), they can be used to obtain the sensitivity of bus voltage to load change.

In the process of defining the voltage stability index, the weakest bus is identified first . Apparently, the weakest bus is the one that is closest to the turning point or "knee" of the PV curve, since that is where stability is lost for constant power type loads. $Cd\lambda$ is common to all buses, so the relative change dV decides the weakest bus. Equivalently, a weak bus is one that has a large ratio of differential voltage change to change in the total load. The weakest bus is then the one with the largest $-\frac{dV}{Cd\lambda}$ ratio. Or, if the ith bus is the weakest bus, then

$$\left|\frac{dV_i}{Cd\lambda}\right| = \max\left\{\left|\frac{dV_1}{Cd\lambda}\right| \quad \left|\frac{dV_2}{Cd\lambda}\right| \quad \cdots \quad \left|\frac{dV_n}{Cd\lambda}\right|\right\}$$

Since $Cd\lambda$ is common to each term, the weakest bus is the one with the largest dV component. Therefore, the weak areas can be easily identified by merely looking at the largest dV component in the tangent vector.

When ith bus reaches its steady state voltage stability limit, the ratio of $-\frac{dV_i}{Cd\lambda}$ becomes infinite, or equivalently the ratio $-\frac{Cd\lambda}{dV_i}$ is zero. Therefore the ratio $-\frac{Cd\lambda}{dV_i}$ is defined as the voltage stability index for the system. This index will be high when the weakest bus is far from instability, but will be zero when the weakest bus reaches voltage collapse. The use of the negative sign guarantees that the index is positive before the critical point is encountered and negative afterwards.

The index is applied to the New England 30-bus test system as well as the 162-bus Iowa reduced system. Figures 4.1 and 4.2 show the trajectories of the voltage stability index for the two system respectively as the load parameter is increased from zero to the critical point. As can be seen, the index is positive before the critical point is reached and decreases to zero at the critical point. However, as can be seen from the graph, this index is

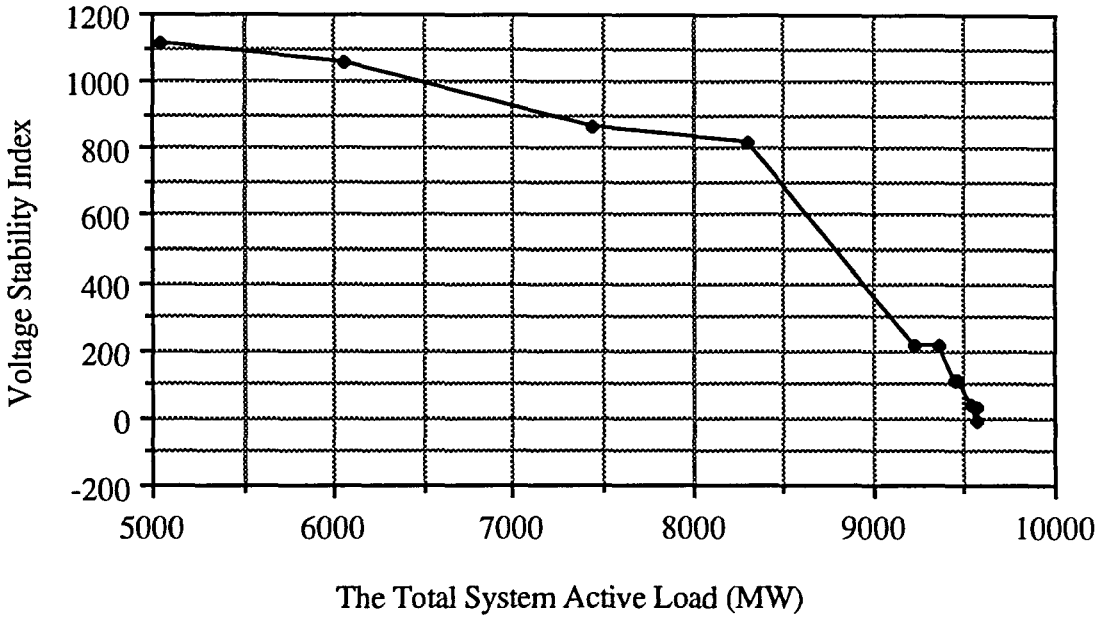

Figure 4.1: The total system active load vs the voltage stability index (30-bus system)

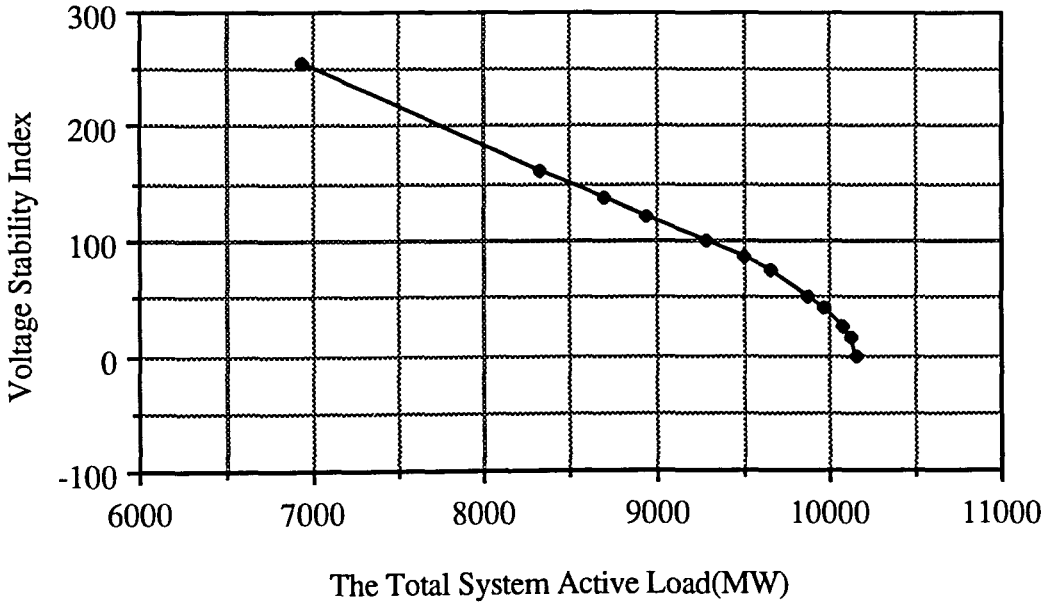

Figure 4.2: The total system active load vs the voltage stability index (162-bus system)

highly nonlinear with respect to the load parameter. Therefore it is unclear how to interpolate between the points on the graph. Furthermore, when the index is reduced to half, it does not mean that the distance to voltage collapse is reduced to half.

4.3 Minimum Singular Value of Jacobian Matrix

Tiranuchit et al. [12] and Löf et al. [13] recently proposed the use of the minimum singular value of the power flow Jacobian matrix as an indicator of the distance to steady-state stability limit. Let x denotes the vector of bus voltages and angles and λ denote the load change parameter. Then the steady-state power flow equation is written in the form:

$$f(x,\lambda) = 0$$

Let dx be the differential change in voltage because of a differential change $d\lambda$ in load. Then by differentiating the above equation, we have

$$Jdx + f_\lambda d\lambda = 0$$

where J is the power flow Jacobian Matrix and $f_\lambda = \frac{\partial f}{\partial \lambda}$. Solving for dx gives

$$dx = -J^{-1} f_\lambda d\lambda$$

$$\|dx\| \le \sigma_1(J^{-1}) \|f_\lambda\| \cdot |d\lambda|$$

where σ_1 represents the largest singular value. Therefore, $\sigma_1(J^{-1})$ determines how large the bus voltage change can be when the load is changed by $d\lambda$. Near the critical point, a small load increase can lead to a very large voltage drop, i.e., $\sigma_1(J^{-1})$ will be very large. But

$$\sigma_1(J^{-1}) = \sigma_n(J)$$

where $\sigma_n(J)$ is the smallest singular value of J. Therefore, $\sigma_n(J)$ becomes very small near the critical point and is equal to zero at the critical point, and can be used to indicate the distance to the critical point.

We have applied the minimum singular value of the power flow Jacobian to the New England 30-bus test system. Figure 4.3 shows the trajectory of $\sigma_n(J)$ as the load change parameter λ is increased from zero to the critical value. As can be seen, $\sigma_n(J)$ decreases as λ is increased and it becomes zero when λ reaches the critical value. However, the amount of decrease is very small during the load increase, and drops very sharply to zero when λ approaches the critical value. Therefore, for large systems, $\sigma_n(J)$ is not a good indicator of the distance to voltage instability. Besides, even for a small system, the nonlinearity of the $\sigma_n(J)-\lambda$ curve introduces difficulty in interpolating between points on the curve and in using $\sigma_n(J)$ as a measure of the distance to voltage collapse. Furthermore, since $\sigma_n(J)$ is a non-negative function of λ, when λ is increased beyond the critical point, $\sigma_n(J)$ gives a positive number, a misleading piece of information.

4.4 Margins to Voltage Instability

The most natural definition of margins to voltage instability would be the distance between the current operating point and the critical point where voltage stability is lost. This distance is more easily measured in the load space, i.e., the distance from the current load to the critical load. To quantify this, two distances can be used: the active power distance ΔP (MW distance) to voltage collapse:

$$\Delta P = P_c - P_o$$

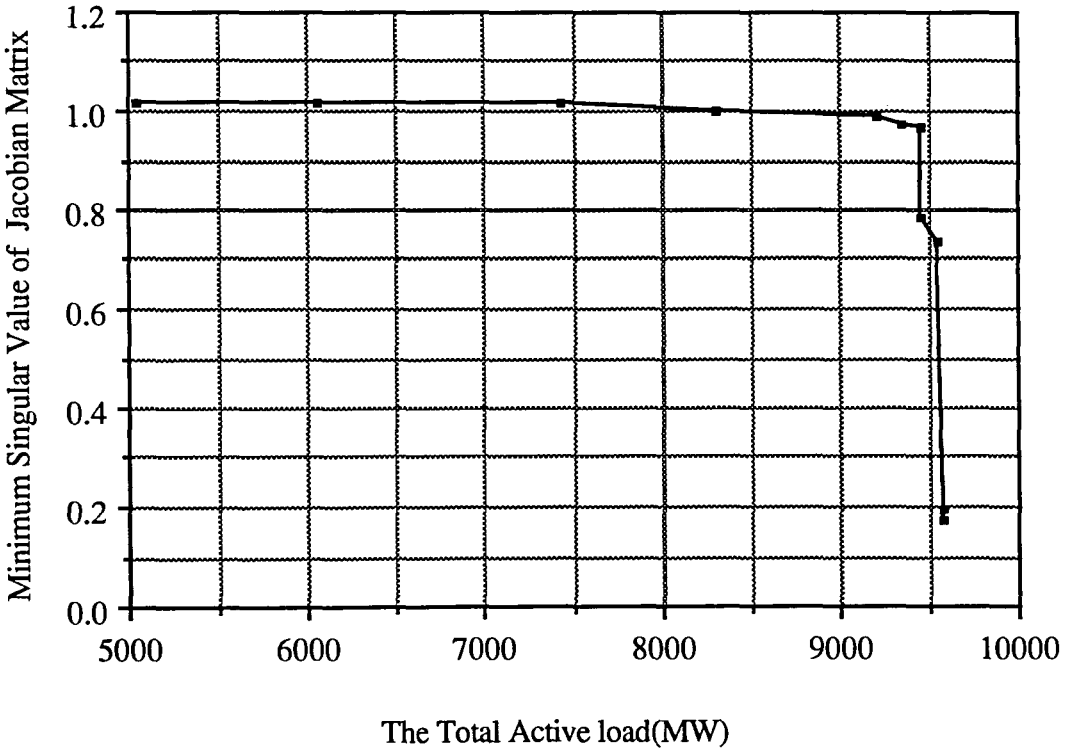

Figure 4.3: Minimum singular value of Jacobian matrix vs the total system active load (30-bus system)

and the reactive power reserve (MVAr) distance ΔQ to voltage collapse:

$$\Delta Q = Q_c - Q_o$$

where P stands for active power and Q stands for reactive power, c stands for the critical point and o stands for the initial point.

Since the margins of the system are different for different contingencies, we need to select the most severe contingency. This involves a standard contingency analysis with techniques available for screening and ranking candidate contingencies. Then we choose the state after the severe contingency as the base case, and add active load (or reactive load or both) until the system becomes unstable. This process can be easily carried out in the

continuation power flow method. At each iteration n of the continuation power flow, we will record the amount of active load increase ΔP^n and reactive power reserve decrease ΔQ^n. They can be calculated as:

$$\Delta P^n = P_n - P_{n-1}$$

and

$$\Delta Q^n = Q_n - Q_{n-1}$$

Once the critical point is reached, the MW-distance and MVAr-distance can be calculated :

$$\Delta P = \sum_{n=1}^{n_{step}} \Delta P^n$$

$$\Delta Q = \sum_{n=1}^{n_{step}} \Delta Q^n$$

where n_{step} is the number of steps in the continuation power flow before the critical point is reached. Either ΔP or ΔQ, or the combined effect of both, can be used as the margin to voltage instability.

4.5 Simulation Results and Comparisons

The margins to voltage instability defined in the last section are tested using the New England 30-bus test system and 162-bus Iowa reduced system. The load increase is shared among the system's generators according to their initial generating ratio. The load is increased until the system reaches the critical point. The continuation power flow method traces a solution path for various load levels. The margins for all load levels are calculated according to the formulae in the previous section. Figures 4.4 and 4.5 show the

MW distance and the reactive power reserve versus the total system active load respectively for the 30-bus system. Figures 4.6 and 4.7 are similar graphs for the 162-bus system.

From these graphs, it can be seen that both MW distance and the reactive power reserve monotonically decrease as the total system active load is increased. They both become zero when the critical point is reached. The behavior of the reactive power reserve is somewhat similar to the voltage stability index and the minimum singular value of the Jacobian matrix in the sense that it is nonlinear with respect to the load change. However, the reactive power reserve curve is much smoother and is apparently decreasing even for low values of load, unlike its opponents, which are insensitive at low load values. Therefore, the reactive power reserve can provide useful information for all load levels and is a better candidate for measuring margins to voltage instability.

The MW distance has even better performance. From Figures 4.4 and 4.6, it is seen that the MW is linear function of the total system active load. Therefore, it is not necessary to calculate all the points on the curve. Once we have found two points on the curve, we can easily find the margin to voltage instability of any operating point by a very simple interpolation. Furthermore, this linearity allows easy comparison of different margins, i.e., if operating point A has a margin twice as large as that of operating point B, then point A is twice as far from voltage collapse as point B. Since the MW distance is equally sensitive to load changes at all load levels, it provides useful information about voltage stability at all load levels.

Note that in this approach, we have to find the critical point before we can calculate the margin to voltage instability. Also, since different load change directions correspond to different critical points, the margins we calculate are dependent on load change directions.

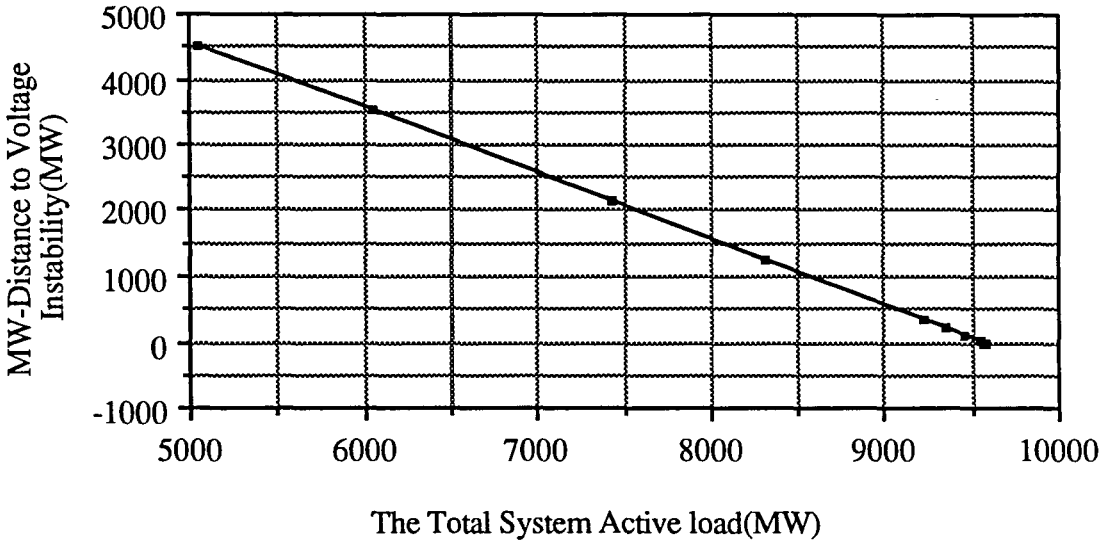

Figure 4.4: The total active load vs the MW-distance to voltage instability (30-bus system)

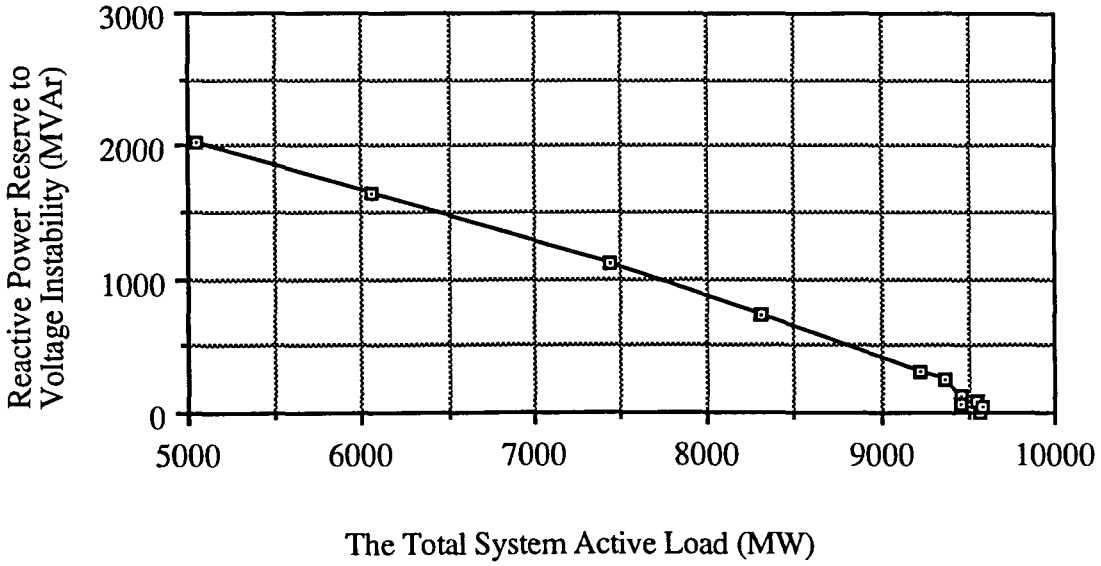

Figure 4.5: Reactive power reserve vs the total system active load (30-bus system)

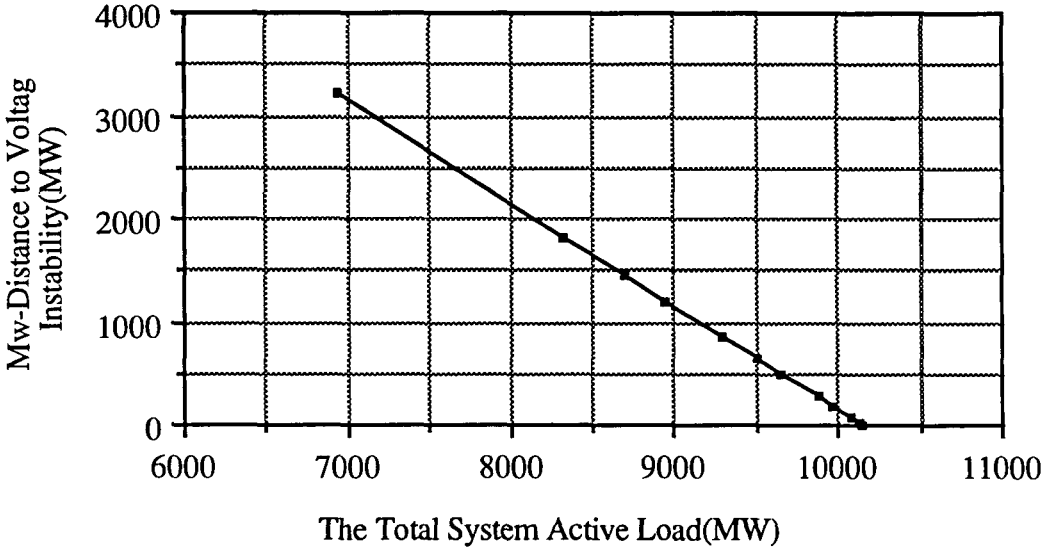

Figure 4.6: The total active load vs the MW-distance to voltage instability (162-bus system)

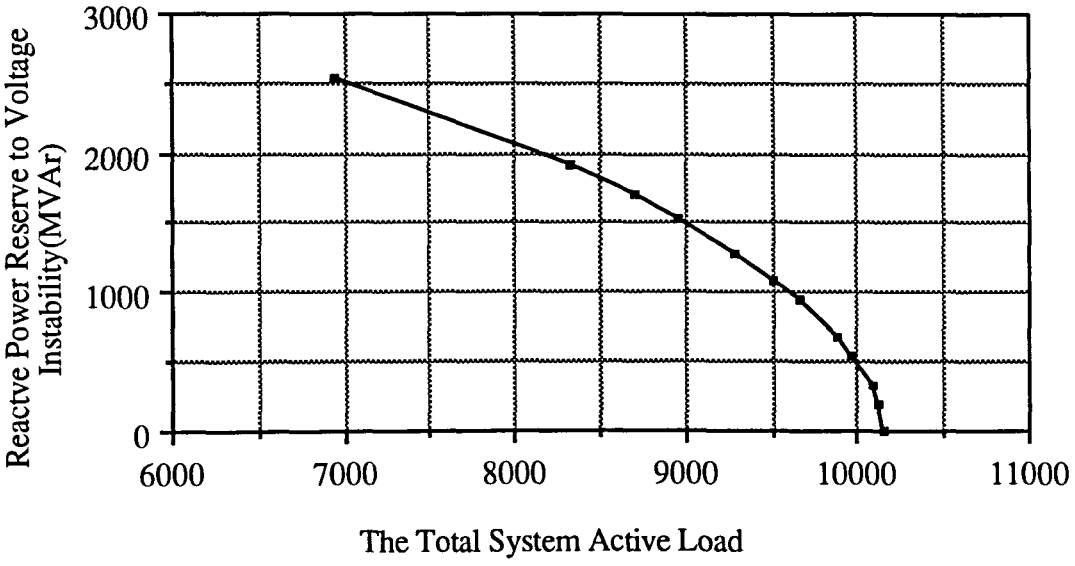

Figure 4.7: Reactive power reserve vs the total system active load (162-bus system)

For a given system and operating point, there is always a particular load change direction that gives the minimum amount of load increase in MW that leads to voltage collapse. If we can somehow find this direction, then load increase in any direction below this minimum amount assures voltage stability. How to find this direction is explained in the next chapter.

CHAPTER 5. WORST CASE DISTANCE TO VOLTAGE STABILITY BOUNDARY

5.1 Introduction

In an electric power network, the solution to the static load flow equation forms a stable equilibrium (operating) point. This equilibrium point x_0 is determined by the load P_0. As the load is increased, the equilibrium point moves toward the critical point, until finally it disappears in a saddle node bifurcation when the load reaches the solvable/unsolvable boundary at P_1. The continuation power flow is capable of finding this critical load if a load change direction is assumed. In the last chapter, it was shown that the difference between the critical load and the current operating load can be used as a good measure of voltage stability margin. However, if the actual load change direction is different from the one used in the continuation power flow, the power system may lose stability before the load is increased by the amount of margin. This is because the actual load change direction is more severe than the assumed one. This can be prevented if we can find the closest point on the solvable/unsolvable boundary, since this point will give us the worst case stability margin. Hence whenever the load increase is less than the worst case margin, the power system is guaranteed to be stable.

The objective of this chapter is to develop a procedure for finding the worst case stability margin. We present an iterative approach and use examples to demonstrate the

method. The key point of this procedure is to find the worst case load change direction. Dobson [15] showed that this worst case load change direction is normal to the solvable/unsolvable boundary. However, in his approach, he did not consider the generator reactive power limits. We incorporated this methodology into our continuation power flow with consideration of the reactive power generation limit. The derivation of the formula to calculate the normal vector as proposed [16-18] is given in the next section. Section 5.3 discusses the calculation of the worst case margin. In Section 5.4, these concepts are tested by applying to the power system examples.

5.2 Normal Vector of the Solvable/Unsolvable Boundary

In the static power system model, the load flow equation includes the real power balance

$$f_1(x,P)=0 \tag{5.1}$$

and the reactive power balance

$$f_2(x,Q)=0 \tag{5.2}$$

where f_1 and f_2 are smooth functions of x, Q and P. Here $x=\begin{pmatrix} V \\ \theta \end{pmatrix}$ is the vector of the bus voltages and voltage angles. The system load is $S=\begin{pmatrix} P \\ Q \end{pmatrix} \in R^m$, where P is the vector of real loads and Q is the vector of reactive loads. The two power balance equations can be combined as the power flow equations

$$f(x,S)=0 \tag{5.3}$$

This power flow equation may or may not admit a real solution for x, depending on the value of the load vector S. If a real vector x can be solved from equation (5.3), we say

that S is a solvable load; otherwise, we say that S is an unsolvable load. Then, all those unsolvable points form an open region in the load vector space R^m, and all those solvable points form a closed region. The boundary between these two regions is a smooth $m-1$ dimensional hyper surface, denoted by Σ. The points on Σ are called critical loads. For such loads, the corresponding solution to the load flow equation is a critical point where a saddle node bifurcation occurs. Therefore, the Jacobian matrix at such a point is singular. Let S_{1c} be a point on Σ and x_1 the corresponding solution. Then

$$f(x_1, S_{1c}) = 0 \tag{5.4}$$

and $f_x(x_1, S_{1c})$ is singular. Here f_x denotes the Jacobian matrix of f with respect to x. Since f_x is singular there exists a non zero vector w such that

$$w^T f_x(x_1, S_{1c}) = 0 \tag{5.5}$$

That is, w is a left eigenvector of the Jacobian f_x associated with the zero eigenvalue. Let dS be tangent to Σ at S_{1c}. Then, from equation (5.4), dS satisfies

$$f_x(x_1, S_{1c})dx + f_S(x_1, S_{1c})dS = 0 \tag{5.6}$$

for some small dx, if dS is small enough. Multiplying equation (5.6) from the left by w^T, we get

$$w^T f_x(x_1, S_{1c})dx + w^T f_S(x_1, S_{1c})dS = 0$$

Using equation (5.5), we obtain

$$w^T f_S(x_1, S_{1c})dS = 0$$

that is,

$$f_S{}^T(x_1, S_{1c})w \perp dS$$

Therefore $f_S{}^T(x_1, S_{1c})w$ is normal to Σ at S_{1c}. This suggests the following procedure for finding the normal vector of the solvable/unsolvable boundary at S_{1c}:

1. Solve the load flow equation (5.4)

2. Find the Jacobian $f_x(x_1, S_{1c})$
3. Find the left eigenvector of $f_x(x_1, S_{1c})$ associated with the zero eigenvalue
4. Find $f_S(x_1, S_{1c})$
5. Let $n = f_S^T(x_1, S_{1c})w \Big/ \left\| f_S^T(x_1, S_{1c})w \right\|$.

Although the above formula was derived in [16-18], our approach is much straightforward and much easier.

5.3 Worst Case Stability Margin

In the continuation power flow method, an initial solvable load S_0 is given and we let

$$S = S_0 + \lambda C$$

where C is a vector of load change direction. We let λ increase until $S = S_1$ reaches the critical boundary. Then the distance between S_1 and S_0 is used as a stability margin for the initial operating point. Hence, this margin is the distance from S_0 to a critical point on the boundary Σ. Let S_* be the closest point from S_0 to the critical boundary. Since Σ is smooth locally around S_*, there is a tangent plane at S_*. Since S_* minimizes the distance of Σ to S_0, $S_* - S_0$ must be perpendicular to the tangent plane of Σ at S_*, that is $S_* - S_0$ must be in the direction of the normal vector n_* of Σ at S_*. Hence

$$S_* - S_0 = \lambda_* n_*$$

$$S_* = S_0 + \lambda_* n_*$$

This suggests that we can find S_* iteratively as follows. Take an initial guess of n_* to be n_0 and this n_0 can be quite arbitrary. Then we can use n_0 as the vector of load change di-

rection in the continuation power flow method to reach the boundary Σ at S_1 along the direction of n_0. Once we have S_1, we can use the procedure outlined in the last section to calculate the normal vector n_1 of Σ at S_1. Then we use this normal vector n_1 as the new estimate of n_* and the new vector of the load change direction. This process continues until we get a convergent solution S_*.

To check for convergence, we can check the direction of the normal vector in each step. If it no longer changes direction any more, that means we have reached the closest point S_* on Σ to S_0. Let n_{k-1} and n_k be the normal vector in the $(k-1)th$ and the kth iteration. The angle between n_k and n_{k-1} can be derived as follows: Construct a triangle as in Figure 5.1.

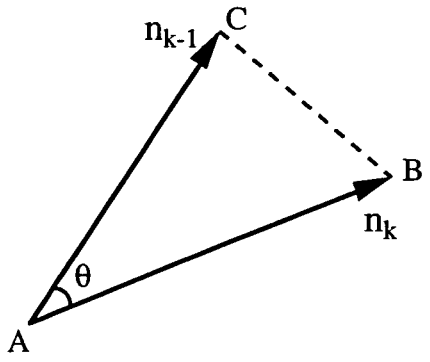

Figure 5.1: Angle between normal vectors

The cosine theorem gives

$$\overline{BC}^2 = \overline{AB}^2 + \overline{AC}^2 - 2\overline{AB}\cdot\overline{AC}\cos\theta$$

Therefore

$$\|n_k - n_{k-1}\|^2 = \|n_k\|^2 + \|n_{k-1}\|^2 - 2\|n_k\|\cdot\|n_{k-1}\|\cos\theta$$

$$\begin{aligned}\|n_k - n_{k-1}\|^2 &= (n_k - n_{k-1})^T (n_k - n_{k-1}) \\ &= n_k{}^T n_k - 2n_k{}^T n_{k-1} + n_{k-1}{}^T n_{k-1} \\ &= \|n_k\|^2 - 2n_k{}^T n_{k-1} + \|n_{k-1}\|^2\end{aligned}$$

Hence

$$-2n_k{}^T n_{k-1} = -2\|n_k\| \cdot \|n_{k-1}\| \cos\theta$$

$$\therefore \quad \cos\theta = \frac{n_k{}^T n_{k-1}}{\|n_k\| \cdot \|n_{k-1}\|}$$

when n_k is very similar to n_{k-1}, θ is very small, $\cos\theta$ is very close to 1.

Therefore, the procedure for finding the worst case stability margin (of an initial load S_0) can be given as follows [15]:

1. Let $k = 0$, select n_0
2. $k = k + 1$
3. Find the critical point S_k by solving the continuation power flow for

$$S_k = S_0 + \lambda n_{k-1}$$

4. Find n_k at S_k, using the procedure in the last section
5. If $\dfrac{n_k{}^T n_{k-1}}{\|n_k\| \cdot \|n_{k-1}\|} < 1.0$, go to 2
6. $\|S_k - S_0\|$ is the worst case stability margin and n_k is the worst case load change direction.

This procedure is graphically illustrated in Figure 5.2

This procedure works quite satisfactorily, especially when the initial load is not too far from the critical boundary. In such cases, the load need not be increased very much when a critical point is encountered. Thus, what we are dealing with is the local behavior

of the critical boundary. Since the boundary is locally smooth, the convergence property of the iteration is nice. Although the above iterative procedure is meant to find the local minimum of the margin, in such cases this local minimum is likely to be the global minimum.

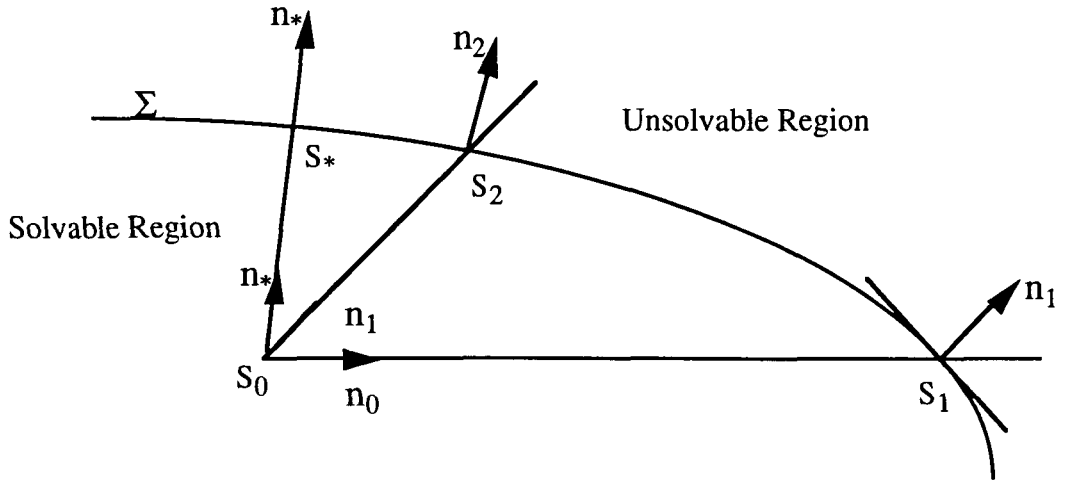

Figure 5.2: Iterative procedure to find worst case load change direction

However, when the initial load is not so small, the situation may possibly be quite different. Since in such cases the voltage stability margin is large, the load needs to be increased greatly before a critical point is encountered. Therefore, the distance between the initial load and the critical point is larger when compared to the curvature of the critical surface. First of all, the local minimum we are going to find is no longer likely to be the global minimum. Even worse, we may not be able to find a local minimum. Figure 5.3 on the following page illustrates one such (imaginary) situation.

5.4 Simulations

In this section, we provide simulation results using the procedures developed in Sections 2 and 3. We first present the simulation results for a 5-bus system in Figure 5.3 as studied in [19]. Then we will present simulation results for the 30-bus New England test system as shown in Figure 5.4.

The system load S_0 at the initial operating point is given in the first row of Table 5.1. We arbitrarily select a load change direction vector n_0 as shown in row 2. Then the procedure outlined in the previous section is followed. The procedure converged in 9 steps. The eight intermediate critical loads and normal vectors together with the final worst case critical load are listed in the remaining rows. The real power margins in each iteration

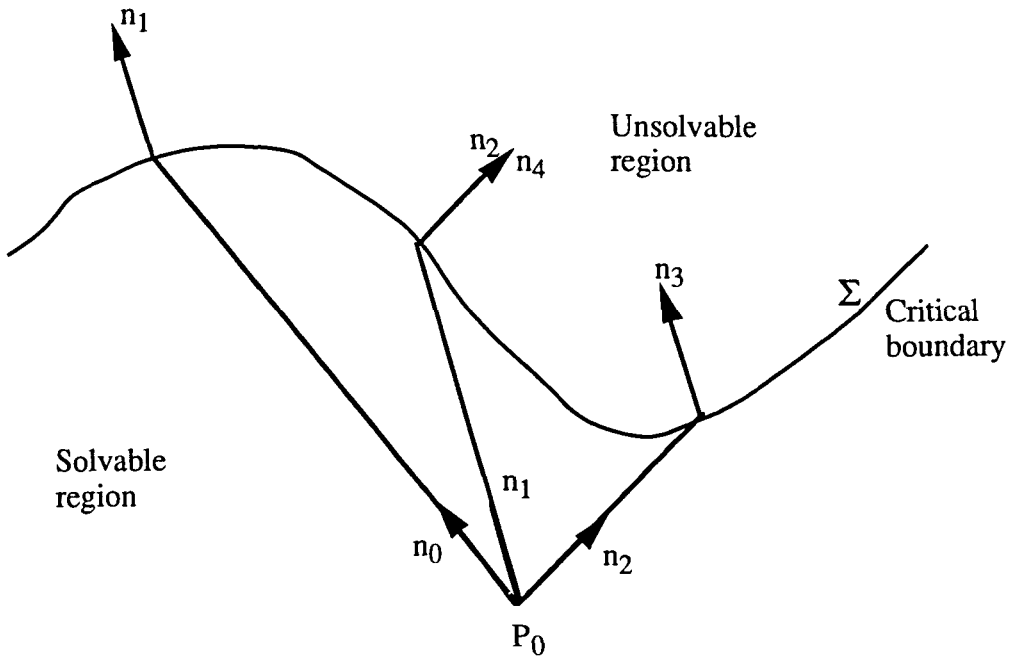

Figure 5.3: Worst case margin may not be found by the proposed iteration

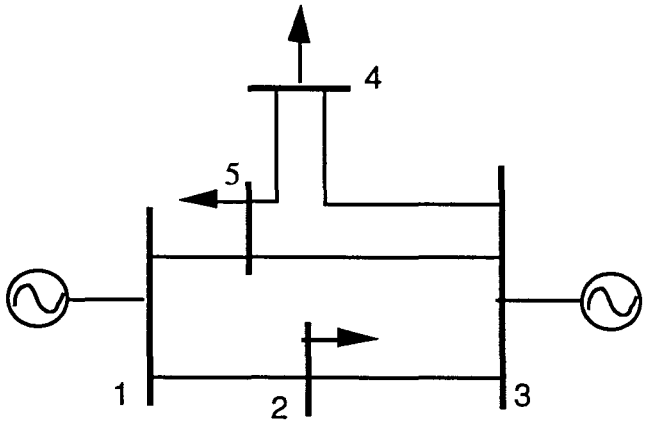

Figure 5.4: 5-bus system

are given in the last column. As can be seen, the margin decreased monotonically as the number of iterations is increased. Also, the normal vector converged to a constant vector rather rapidly, which corresponds to the worst case load change direction. The last critical load S_9 is the closest point from the initial load S_0 to the solvable /unsolvable boundary.

This procedure is then applied to the 30 bus New England test system, and convergence is obtained in only four iterations. Table 5.2 lists the initial system load, the three intermediate critical loads, and the final worst case critical load. The real power margins in each iteration are also listed in the last row. Although the final margin is a slightly larger than the preceding one, the difference is less than 0.04 percent of the initial system load. Therefore, we can consider the last two margins the same. This small error is expected to be reduced if we select a stricter convergence criterion.

Table 5.3 contains the initial load change direction and normal vectors at the critical loads of Table 5.2. Although it seems that n_3 and n_4 are quite different, they actually represent almost the same direction (the angle between the two is less than 2 degrees). The

reason is that they are not unit vectors; rather, they have been scaled to satisfy a requirement on the load change direction vector [3] in the continuation power flow method.

Besides providing the worst case load change direction and worst case voltage stability margin, the procedure can also be used to identify buses with the heaviest load sharing. Figures 5.5 and 5.6 show the five largest real load buses, corresponding to S_0 and S_4, respectively. In each figure, the Roman numerals I, II, III, IV, V by the buses represent the rank of the five largest active loads. Note that the two buses with the heaviest load sharing remain the same. However, the relative ranks of the third, fourth, and fifth largest load sharing buses are rotated.

During the simulation, one special concern needs to be taken care of. Since the new load change directions are calculated from the left eigenvector of the Jacobian matrix, the components may be positive or negative. For a negative component, the corresponding bus experiences an actual load decrease as the total system real power load is increased. This may cause the real load at some buses to become negative. Since a negative real load is physically impossible, physical constraints must be set to prevent the real load from becoming negative. This is done by simply setting the corresponding negative component to zero in the load change direction vector when the real load approaches zero at a bus.

Once the worst case margin is found, it can be used to assess power system security. If the worst case margin is smaller than a certain threshold, the system is operating dangerously close to voltage instability. Load shedding measures must be taken to ensure voltage stability. For certain contingencies, the margin may be completely lost and the total system load is too large to be solvable. The method in this chapter is no longer useful. The next chapter presents an optimal load shedding strategy to deal with such cases.

Table 5.1: Initial and critical loads and normal vector in 5-bus system

	p_2	q_2	p_4	q_4	p_5	q_5	$\|S_i - S_0\|_1$
S_0	1.1500	0.6000	0.7000	0.3000	0.7000	0.4000	
n_0	0.3513	0.0055	0.7160	-0.0326	0.3570	0.0074	
S_1	1.8219	0.6105	2.0694	0.2377	1.3828	0.4142	2.720
n_1	-9.7934d-3	-5.8608d-5	0.7372	0.6500	8.0119d-2	0.1650	
S_2	1.1409	0.5999	1.3862	0.9049	0.7746	0.5536	0.7500
n_2	2.0342d-3	1.0885d-4	0.5775	0.8005	5.6537d-2	0.1499	
S_3	1.1518	0.6001	1.2149	1.0137	0.7504	0.5336	0.5700
n_3	-4.9995d-3	-3.1683d-4	0.5106	0.8479	3.8600d-2	0.1368	
S_4	1.1455	0.5997	1.1561	1.0575	0.7345	0.5222	0.4900
n_4	-2.9286d-3	-1.8682d-4	0.4960	0.8563	4.1190d-2	0.1381	
S_5	1.1474	0.5998	1.1430	1.0647	0.7368	0.5233	0.4800
n_5	-3.0338d-3	-1.9433d-4	0.4917	0.8588	4.0821d-2	0.1377	
S_6	1.1473	0.5998	1.1391	1.0669	0.7365	0.5229	0.4700
n_6	-3.0437d-3	-1.9533d-4	0.4905	0.8596	4.0715d-2	0.1375	
S_7	1.1473	0.5998	1.1378	1.0676	0.7364	0.5228	0.4700
n_7	-3.0461d-3	-1.9559d-4	0.4901	0.8589	4.0686d-2	0.1375	
S_8	1.1473	0.5998	1.1377	1.0678	0.7363	0.5228	0.4700
n_8	-3.0468d-3	-1.9567d-4	0.4900	0.8589	4.0677d-2	0.1375	
S_9	1.1473	0.5998	1.1377	1.0679	0.7363	0.5228	0.4700

Table 5.2: Initial and critical loads in 30-bus system

	S_0	S_1	S_2	S_3	S_4
p_3	3.2200	6.1061	3.4069	3.3417	3.3232
q_3	0.0240	0.0455	1.1129	1.3644	1.3768
p_4	5.0000	9.8416	5.2622	5.1707	5.1225
q_4	0.8400	1.5929	2.3089	2.2318	2.2070
p_7	2.3380	4.4336	2.5576	2.4851	2.4628
q_7	0.8400	1.5929	2.1848	2.0613	2.0431
p_8	5.2200	9.8987	5.4798	5.3897	5.3638
q_8	0.7600	1.4412	2.0565	1.9354	1.9214
p_{12}	0.0850	0.1612	0.0000	0.0075	0.0259
q_{12}	0.8800	1.6686	2.4804	2.4412	2.3784
p_{15}	3.200	6.0682	3.3960	3.3022	3.2859
q_{15}	1.5300	2.9014	3.4183	3.2641	3.1637
p_{16}	3.2940	6.2465	3.2825	3.2630	3.2818
q_{16}	0.3230	0.6125	2.2078	2.2010	1.9334
p_{18}	1.5800	2.9962	1.7694	1.7026	1.6879
q_{18}	0.3000	0.5689	1.7746	1.8293	1.8189
p_{21}	2.7400	5.1959	2.3563	2.4871	2.5633
q_{21}	1.1500	2.1808	3.2201	2.8767	2.7600
p_{24}	3.0860	5.8520	3.0607	3.0405	3.0632
q_{24}	0.9220	1.7484	2.8982	2.6703	2.5629
p_{26}	1.3900	2.6359	1.3079	1.3592	1.3689
q_{26}	0.1700	0.3224	1.0146	1.5541	1.6853
p_{27}	2.8100	5.3286	2.9126	2.9035	2.9056
q_{27}	0.7550	1.4317	1.9590	2.2871	2.3608
p_{28}	2.0600	3.9064	1.7886	1.8260	1.8268
q_{28}	0.2760	0.5234	0.4808	1.5879	1.8191
$\|P_i - P_0\|_1$		4.5230	0.6400	0.2600	0.2800

Table 5.3: Initial load change direction and normal vectors in 30-bus system

	n_0	n_1	n_2	n_3	n_4
p_3	21.4667	1.2539	1.5995	1.2464	1.1783
q_3	0.1600	8.6459	17.6144	16.3370	14.6187
p_4	33.3333	1.7589	2.2432	1.7215	1.5921
q_4	5.6000	9.8530	18.2895	16.5083	14.6403
p_7	15.5876	1.4729	1.9335	1.5073	1.3638
q_7	5.6000	9.0208	16.0498	14.5300	12.8020
p_8	34.8000	1.7424	2.2307	1.7363	1.5718
q_8	5.0667	8.6965	15.4465	14.0260	12.3523
p_{12}	0.5667	-0.9455	-1.0181	-0.7136	-0.6266
q_{12}	5.8667	10.7351	20.5157	18.0963	15.9498
p_{15}	21.3333	1.3150	1.3430	1.0370	1.0141
q_{15}	10.2000	12.6661	22.7884	19.4512	17.5594
p_{16}	21.9600	-7.7320	-0.4072	-0.1472	-6.4382d-2
q_{16}	2.1533	12.6432	22.3132	19.4511	17.3400
p_{18}	10.5333	1.2703	1.6117	1.3026	1.2559
q_{18}	2.0000	9.8912	20.0965	18.3430	16.4644
p_{21}	18.2667	-2.5740	-3.3237	-2.1340	-1.8734
q_{21}	7.6667	13.8856	22.6907	19.4442	17.2817
p_{24}	20.5733	-0.1695	-0.5973	-0.2749	-0.1740
q_{24}	6.1467	13.2558	22.9753	19.8168	17.6507
p_{26}	9.2667	-0.5504	-0.4048	-0.2546	-0.2326
q_{26}	1.1333	5.6652	18.1877	18.2999	16.8543
p_{27}	18.7333	0.6880	1.2291	1.1540	1.1493
q_{27}	5.0333	8.0764	20.1334	19.3923	17.7303
p_{28}	13.7333	-1.8204	-3.0752	-2.8164	-2.7900
q_{28}	1.8400	1.3740	17.2401	18.6358	17.4613

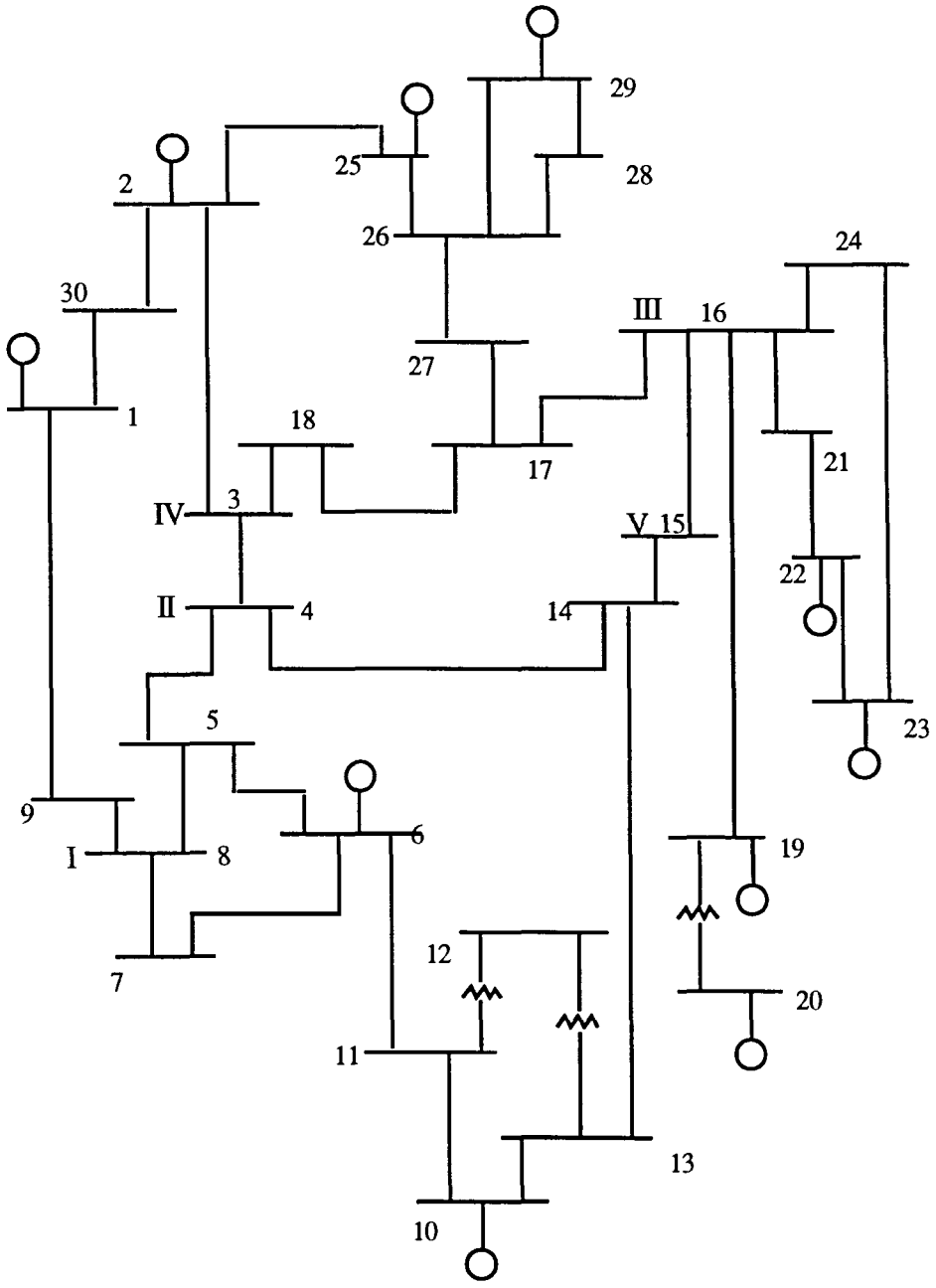

Figure 5.5: 30-bus system with 5 largest load buses identified at S_0

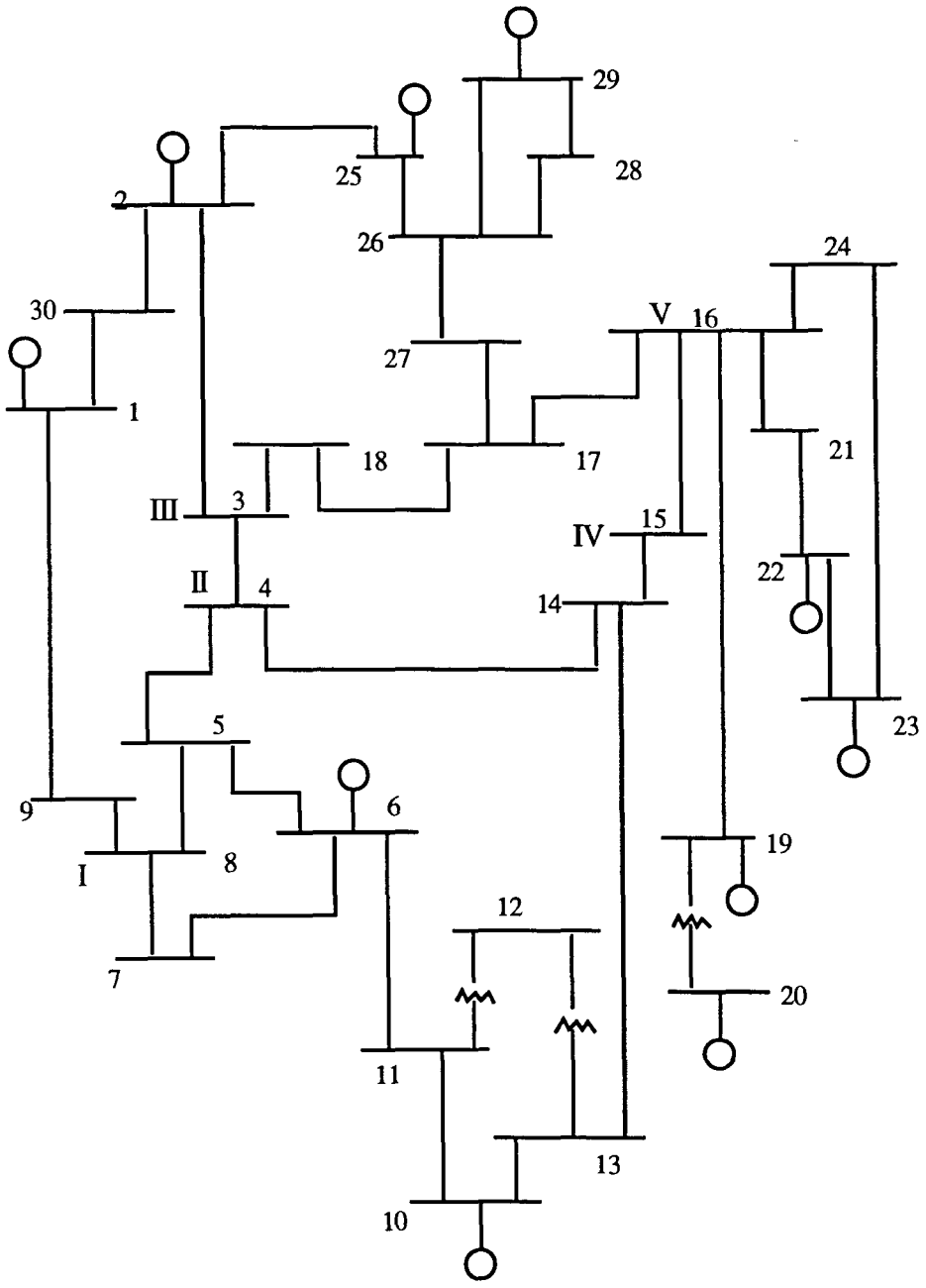

Figure 5.6: 30-bus system with 5 largest load buses identified at S_4

CHAPTER 6. OPTIMAL LOAD SHEDDING FOR UNSOLVABLE LOADS

6.1 Introduction

Up to now, we have been considering the voltage stability problem when the system load is increased from an initial load. The presumption in doing this is that the initial load must correspond to a stable operating point. That is, the power flow equation must have a unique solution. In this chapter, we consider the problem of voltage stability by load shedding when the initial system load is so large that the system can not be operated at a stable operating point. Such a system load is called an unsolvable load, because the power flow equation does not have a solution.

We study this problem because that the unsolvable loads often represent the most severe threats to secure system operation. If we try to operate the system with an unsolvable load, it will lead to voltage collapse. Therefore, it is very important to identify unsolvable loads and to find the best way to decrease the load to insure system stability. Furthermore, these unsolvable loads are not imaginary situations. For example, when contingency occurs, an already stressed system is further degraded through the removal of additional equipment. Then the solvable load before contingency may become an unsolvable load after the contingency.

The objectives of this chapter include the following: 1) to find a suitable method for solving the power flow equation that can be easily incorporated into the continuation power flow method and that can handle both solvable and unsolvable loads, 2) for an unsolvable load, to find the optimal load shedding to regain voltage stability.

The organization of this chapter is as follows. In Section 6.2, we review a method that is very intuitive and can be easily incorporated into the continuation power flow method. But it can not provide guaranteed convergence, especially for the situations in which we are most interested. In Section 6.3, we provide a modified scheme based on the method in Section 6.2, which will now guarantee convergence. In Section 6.4, we introduce an iterative procedure to find the closest point on the stability/instability boundary to an unsolvable load, and thus derive an optimal load shedding method for achieving voltage stability. Simulation results using the continuation power flow package are demonstrated in Section 6.5.

6.2 Damped Newton-Raphson Method in Polar Coordinates

The Newton- Raphson method is used to solve the power flow equation

$$F(x) = 0 \tag{6.1}$$

using the iterative formula

$$x_{k+1} = x_k - \Delta x_k \tag{6.2}$$

$$\Delta x_k = J^{-1} F(x_k) \tag{6.3}$$

where J is the Jacobian matrix evaluated at x_k.

However, in the case of unsolvable loads, this method will not converge, since there is no solution to the power flow equation. In order to get the best approximate solu-

tion to equation (6.1), we can transform the problem of solving a set of nonlinear equations to the problem of minimizing an objective function:

$$\min_x G(x) = [F(x)]^T F(x) \tag{6.4}$$

This vector optimization problem can be further simplified by introducing the so-called "optimal multiplier" in order to change the problem into a scalar optimization problem [20]. The basic idea is as follows. Let

$$x(\mu) = x_k - \mu \Delta x_k \tag{6.5}$$

Then the vector minimization problem in (6.4) becomes a scalar minimization problem.

$$\min_\mu G(\mu) = G(x(\mu)) = [F(x_k - \mu \Delta x_k)]^T F(x_k - \mu \Delta x_k) \tag{6.6}$$

In Cartesian coordinates, the power flow equation is a second order polynomial equation, and the minimization of μ can be obtained by solving a third-order scalar polynomial [20], as discussed in appendix B. In this method, the total mismatch (the objective function) is guaranteed to decrease in each step. For solvable loads, $\mu^* \approx 1$. For unsolvable loads, $\mu^* \to 0$.

Since the continuation power flow method is formulated in the polar coordinates, the optimal multiplier method needs to be transformed into the polar coordinates in order for it to be incorporated into the continuation power flow method. However, even though this transformation is straightforward, once it is in the polar coordinates, the power flow equation becomes nonpolynomial. The higher order terms can no longer be handled analytically. A linearization technique has to be used in order to solve for the optimal multiplier. Because of this approximation, it is no longer guaranteed that the total mismatch will decrease in each N-R iteration. In our simulation, we have observed that oscillation will occur most of the time if the load is in unsolvable range. Furthermore, the computation in-

volved in transforming back and forth between polar and Cartesian coordinates is quite expensive.

Dehnel and Dommel [21] proposed a simpler method, which they called the damped Newton-Raphson method. It is also a Newton/minimization method. Since it is formulated in polar coordinates, it can easily be incorporated into the continuation power flow method.

Suppose that in the *kth* iteration of Newton-Raphson, we have calculated the correction vector Δx_k (here everything is in polar coordinates). In an attempt to find a suitable multiplier $\mu_{\min}$ such that $x_k + \mu_{\min}\Delta x_k$ will minimize the total mismatch $G(x_k + \mu_{\min}\Delta x_k)$, the following steps are used. First, we select an initial guess for $\mu_{\min}$, say, $\Delta\mu$. Then we evaluate $G(x)$ at three points: $\phi_1 = G(x_k - \Delta\mu\Delta x_k)$, $\phi_2 = G(x_k - 0\cdot\Delta x_k)$, $\phi_3 = G(x_k + \Delta\mu\Delta x_k)$. Interpolating these three points, $G(x)$ can be approximated by the following second order polynomial:

$$\phi(\mu) = \phi_2 - \frac{\phi_1 - \phi_3}{2\Delta\mu}\mu + \frac{\phi_1 - 2\phi_2 + \phi_3}{2(\Delta\mu)^2}\mu^2$$

Finally, we will select $\mu_{\min}$ to minimize the above second order function. This $\mu_{\min}$ can be easily calculated to be

$$\mu_{\min} = \frac{\Delta\mu(\phi_1 - \phi_3)}{2\phi_1 - 4\phi_2 + 2\phi_3}$$

As for the selection of $\Delta\mu$, the authors [21] proposed the following formula

$$\Delta\mu = \alpha\mu_{\min}{}^{k}\frac{\left\|\Delta x^{k-1}\right\|}{\left\|\Delta x^{k}\right\|}$$

where α has been suggested to be chosen as $\alpha = 0.25$.

The advantage of this method is that it is simple and intuitive and that it can easily be incorporated into the continuation power flow method, since it is formulated in polar co-

ordinates. However, unlike the method in the Cartesian coordinates, the damped Newton-Raphson method does not guarantee the reduction of the total mismatch in each iteration. The reason is that $\mu_{\min}$ is selected to minimize $\phi(\mu)$, which is an approximation of the total mismatch. Although we will have $\phi(\mu_{\min}) \leq G(x_k)$, we are not guaranteed to have $G(x_{k+1}) = G(x_k + \mu_{\min}\Delta x_k) \leq G(x_k)$. In fact, our simulation has demonstrated that the total mismatch can increase, especially when we are close to the solvable/unsolvable boundary, which is the region in which we are most interested.

6.3 Damped N-R Method with Guaranteed Convergence

In order to obtain a method with guaranteed convergence for the continuation power flow method, we decided to modify the method outlined in the last section. Since the problem is already formulated in polar coordinates, simplicity will be reserved.

The idea behind our modification is quite simple. The divergence problem of the method in the last section is a result of the fact that $\mu_{\min}$ is minimizing $\phi(\mu)$, an approximation of the total mismatch rather than the total mismatch $G(x)$ itself. In order to insure convergence, we select μ out of $\pm\Delta\mu$, 0, $\mu_{\min}$ such that the corresponding G is the minimum. Then the new mismatch is guaranteed to be smaller or equal to the total mismatch in the previous step. Thus the convergence is guaranteed. $\Delta\mu$ is initially selected to be 0.25 from experience and updated in each iteration.

The rules for updating $\Delta\mu$ include three different situations. The first situation is graphically shown in Figure 6.1 where ϕ_4 is the smallest. This means that μ^* is the best step size and $\Delta\mu$ has worked well for the damped Newton-Raphson method. Therefore, we select $\Delta\mu$ in the next step to be the average of μ^* and $\Delta\mu$ of the current step. The

second situation, in which ϕ_2 is the smallest, is graphically shown in Figure 6.2. Since this indicates that 0 is the best step size out of the four choices, $\Delta\mu$ must be too large. Therefore, we reduce $\Delta\mu$ by half. In the third situation, either ϕ_1 or ϕ_3 is the smallest. Figure 6.3 shows the situation where ϕ_3 is the smallest. Since the minimum of the four points happens at the edge, the tentative step size $\Delta\mu$ must be too small. Therefore, we need to increase $\Delta\mu$. We consider two cases: if $\Delta\mu$ is also too small in the previous iteration, we increase $\Delta\mu$ by 100%; otherwise, we increase $\Delta\mu$ by half.

Then the modified damped Newton-Raphson algorithm is as follows:

1. Take the initial $\Delta\mu = 0.25$
2. Evaluate the total mismatch $\begin{cases} \phi_1 = G(x_k - \Delta\mu\Delta x_k) \\ \phi_2 = G(x_k - 0 \cdot \Delta x_k) \\ \phi_3 = G(x_k + \Delta\mu\Delta x_k) \end{cases}$

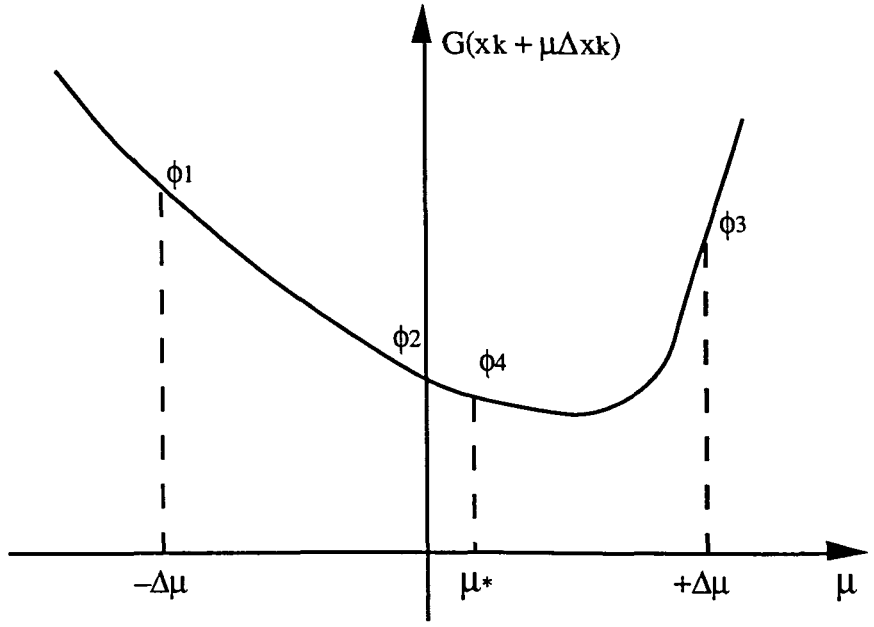

Figure 6.1: Illustration of updating $\Delta\mu$ (Case 1)

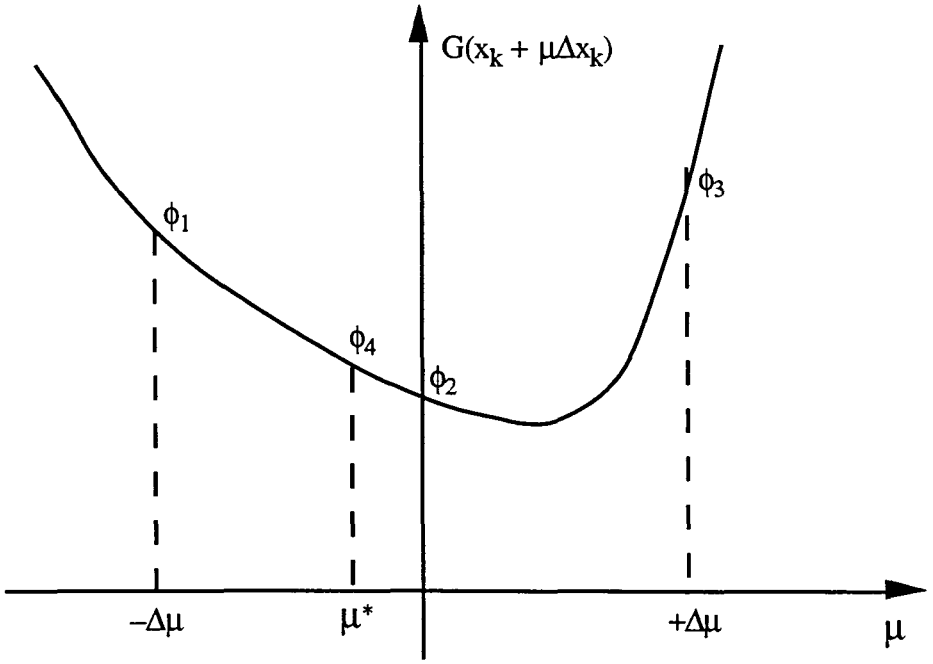

Figure 6.2: Illustration of updating $\Delta\mu$ (Case 2)

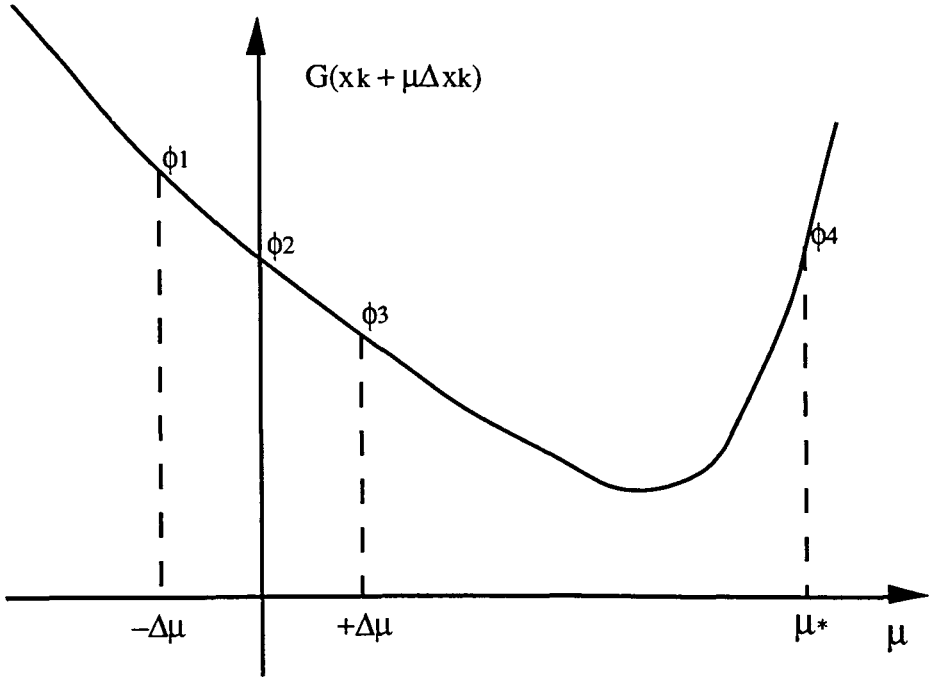

Figure 6.3: Illustration of updating $\Delta\mu$ (Case 3)

3. Compute $\mu = \mu^*$ which minimizes the second order polynomial. i. e.,

$$\mu^* = \frac{\Delta\mu(\phi_1 - \phi_3)}{2\phi_1 - 4\phi_2 + 2\phi_3}$$

4. Evaluate $\phi_4 = G(x_k + \mu^* \Delta x_k)$

5. If ϕ_1 is the smallest, set $\mu = -\Delta\mu$ and, if the previous time ϕ_1 is also smallest,

$$\Delta\mu = 2\Delta\mu \text{; otherwise, } \Delta\mu = 1.5\Delta\mu$$

If ϕ_2 is the smallest, set $\mu = 0$, i. e., no change and $\Delta\mu = \Delta\mu/2$

If ϕ_3 is the smallest, set $\mu = \Delta\mu$, and if ϕ_3 is the smallest last time,

$\Delta\mu = 2\Delta\mu$, else $\Delta\mu = 1.5\Delta\mu$

If ϕ_4 is the smallest, set $\mu = \mu^*$ and $\Delta\mu = \frac{\Delta\mu + \mu^*}{2}$

6. If $\Delta\mu > 1$, $\Delta\mu = 1$; if $\Delta\mu < -1$, $\Delta\mu = -1$

7. $x_{k+1} = x_k + \mu\Delta x_k$, $\Delta x_{k+1} = -J^{-1}F(x_{k+1})$

8. If not converged, $k = k + 1$; go to 2.

9. Done.

Note that in step 6, we have limited $\Delta\mu$ to a maximum of ± 1 to prevent potential divergence. This procedure guarantees that the total mismatch will be decreased at each step, and the solution will converge to a local minimum.

6.4 Optimal Load Shedding to Regain Voltage Stability

In this section, we incorporate the recent results of Overbye [22] into the continuation power flow method in order to provide optimal load shedding to regain voltage stability for unsolvable loads. The optimal load shedding is the minimum amount of the load reduction needed to move an unsolvable load to the solvable region. By optimality, the final

point must be on the solvable/unsolvable boundary, and the vector connecting the initial unsolvable load and the reduced load must be perpendicular to this boundary.

Let P be the vector of the initial unsolvable load and S be the corresponding vector of injection, i.e., the constant real and reactive power load minus generation. Let P^m be the load after the optimal load shedding and S^m be the corresponding injection. Then it can be easily seen that the optimal load shedding $P - P^m$ is the same as $S - S^m$. Therefore our goal is to find a new injection S^m such that 1) S^m is on the solvable/unsolvable boundary, and 2) $S - S^m$ is normal to the boundary.

By using the procedure provided in the last section, the best approximation solution x^* is guaranteed to be a local minimum of the total mismatch $G(x) = [F(x)]^T F(x)$ $= (S - f(x))^T (S - f(x))$. Therefore, x^* must satisfy the necessary condition of local minimum

$$\frac{d}{dx} G(x^*) = \frac{d}{dx}\left[F(x^*)^T \cdot F(x^*)\right]$$
$$= -2J(x^*)^T (S - f(x^*)) = 0$$

Since we have an unsolvable load, $S - f(x^*) \neq 0$. Therefore, $J(x^*)$ is singular, which implies that x^* is on the stability/instability boundary. Hence, $f(x^*)$ corresponds to a load on the solvable/unsolvable boundary Σ. Although this $f(x^*)$ may not be S^m, the projection of $S - f(x^*)$ onto the normal of Σ at $f(x^*)$ can be used as an approximation of the optimal load shedding. Since, by a result of Dobson [15], the left eigenvector w corresponding to the zero eigenvalue of $J(x^*)$ is perpendicular to the boundary, the following formula can be used to calculate S^m:

$$S^m = S - ((S - f(x^*))^T w) w$$

This suggests the following iterative procedure [22]:

1. Set $S^0 = S$, $i = 0$, select tolerance ε

2. Solve: $\min(S^i - f(x))^T (S^i - f(x))$, to get x^{i*}
3. If $\|S^i - f(x^{i*})\| \leq \varepsilon$, go to 7
4. Calculate left eigenvector w^i corresponding to the zero eigenvalue of $J(x^{i*})$
5. Let $S^{i+1} = S - ((S - f(x^{i*}))^T w^i) w^i$
6. Let $i = i + 1$, go to 2
7. Optimal load shedding $= S - S^i$
8. Done

This procedure is graphically illustrated in Figure 6.4. Note that S^0 is the initial injection, which lies in the unsolvable region. By solving the minimization problem in step 2 using the method from the previous section, we land on a point $f(x^{0*})$ on the solvable/unsolvable boundary Σ. By projecting along the normal vector at this point, we obtain a new injection S^1. Repeating step 2, we arrive at another point on the boundary Σ. This process continues until the injection converges to the closest point S^m on Σ to S^0 .

6.6 Simulation

We have applied the optimal load shedding procedure of the previous section to the 30 bus New England test system and the 162-bus Iowa reduced system described in Chapter 3. In doing so, we have paid special attention to the performance of the damped Newton-Raphson method with guaranteed convergence, which was presented in Section 6.4. The simulation results are summarized in the following several tables.

Table 6.1 illustrates the simulation results for the 30 bus England test system. The load is a solvable load. As can be seen from the table, the total mismatch is strictly reduced in each step until it converges to zero, indicating that a convergent solution has been found.

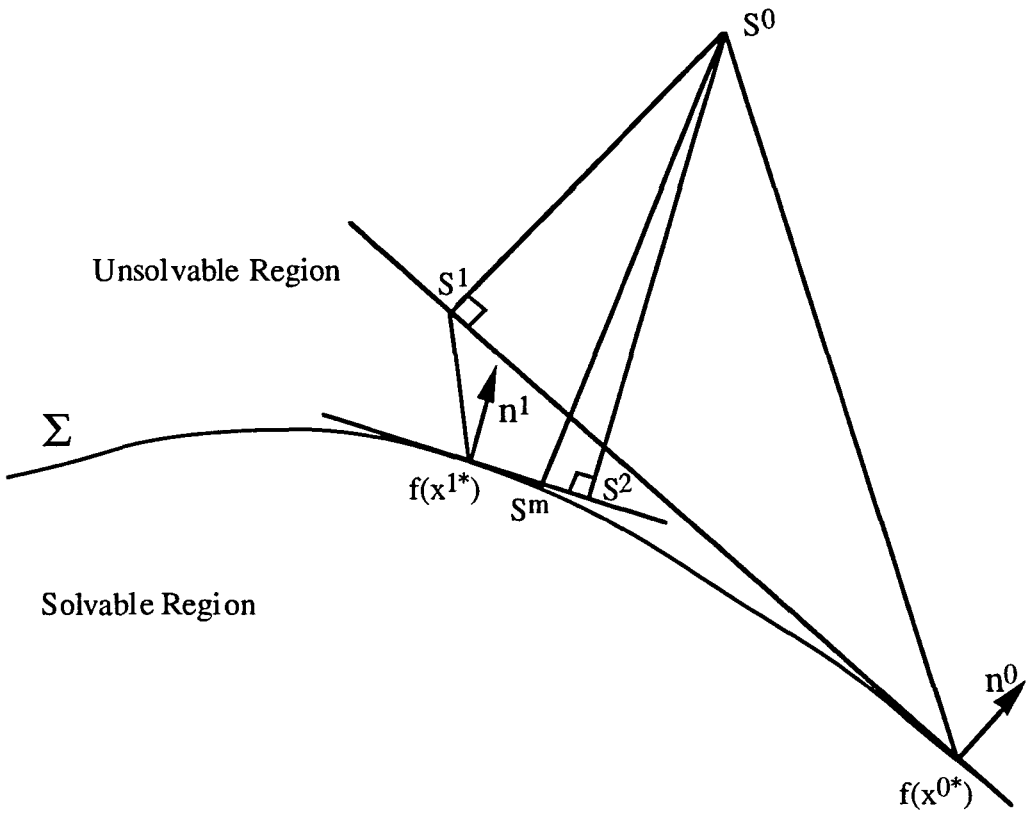

Figure 6.4: Illustration of the iterative procedure for optimal load shedding

Table 6.1: Performance of damped N-R method with guaranteed convergence (30-bus system)

Iteration Number	Total Mismatch	Choice of Multiplier
1	1.857	$+\Delta\mu$
2	0.936	$+\Delta\mu$
3	0.238	$+\Delta\mu$
4	0.000	$+\Delta\mu$

Thus, this method can handle the solvable case rather efficiently. We have also compared the resulting solution with that obtained by a standard method, and voltage solutions are the same. One point we would like to point out is that in all five steps, the multiplier has been selected to be $+\Delta\mu$, instead of $\mu_{\min}$. This means that $\mu_{\min}$ as proposed by Dehnel and Dommel [21] did not provide as much mismatch reduction as $+\Delta\mu$. Therefore, $\mu_{\min}$ does not represent an "optimal multiplier". In our experience, this has usually been the case.

Table 6.2 illustrates the simulation result for the same 30 bus system but with a different (increased) load. For this load, the iteration converged to a solution whose corresponding total mismatch is not zero, meaning that we have an unsolvable load. It has also been verified that the Jacobian matrix at the final solution has an eigenvalue which is several order of magnitude smaller than the rest of the eigenvalues. This verifies that the iteration has converged to a local minimum. From the table, it can also be seen that the total mismatch is reduced in each step, except when there is PV-PQ bus change, where we see a large change in the total mismatch. The reason for this is that when PV-PQ change happens, the system dimension is changed and, therefore, whatever solution we have arrived is expected to be away from the final solution. Again, we see in this example that the $\mu_{\min}$ does not often correspond to the best total mismatch reduction. As a matter of fact, if we have selected $\mu_{\min}$ as the optimal multiplier in each step for this example, the iteration would have become divergent. This explains why we have proposed the modification.

Table 6.3 summarizes the performance of the optimal load shedding procedure as applied to the 30-bus test system. First, note that the total mismatch is reduced in each iteration until finally it converges to zero. This implies that the injection obtained by projec-

Table 6.2: Performance of damped N-R method with guaranteed convergence (162-bus system)

Iteration Number	Total Mismatch	Choice of Multiplier
1	11.989	$+\Delta\mu$
2	6.643	$+\Delta\mu$
3	3.338	$+\Delta\mu$
4	1.374	$+\Delta\mu$
5	0.365	$+\Delta\mu$
6	0.071	$+\Delta\mu$
7	0.006	$+\Delta\mu$
PV-PQ Changed		
8	16.506	0
11	12.667	$+\Delta\mu$
13	4.342	$+\Delta\mu$
17	3.555	$+\Delta\mu$
23	3.539	$+\Delta\mu$
27	3.520	$+\Delta\mu$
32	3.518	μ_{min}
33	3.517	$+\Delta\mu$

tion in each iteration, is finally moved from the unsolvable region to the boundary Σ. Secondly, the minimum eigenvalue of the Jacobian matrix is quite small, indicating that in each iteration the damped N-R method has provided convergent solution on the boundary. Finally, the last row shows the amount of the load shedding needed to regain voltage sta-

bility in each step. In this example, this number is reduced in each step until it finally became a minimum. This minimum is the optimal (minimum) load shedding for stability.

Table 6.4 contains the simulation result using the same procedure but for a much larger, 162-bus Iowa reduced system. Note that unlike our results in the previous example, we do not have uniform decreasing of the total mismatch, or the load shedding, although the damped N-R method still produces a solution on the boundary in each step.

Table 6.3: Testing results on optimal load shedding (30-bus system)

Iteration Number	$\|S^i - f(x^{i*})\|_2$	Min Eigvl	$\|S^0 - f(x^{i*})\|_2$
1	3.134	$-2.925*10^{-6}$	3.558
2	1.012	$-3.158*10^{-3}$	1.934
3	0.363	$-1.158*10^{-4}$	1.672
4	0.138	$6.559*10^{-2}$	1.627
5	0.0001		1.627

This can be explained as follows. For a large system, when the load (or injection) is close to the critical point (or the boundary), it is likely that some generator may have hit its reactive power reserve limit, or at some bus the calculated load became negative. Our software automatically takes care of such incidents by imposing necessary limit bounds on the load and reactive power reserve. However, the use of such bounds includes a non-smooth operation. Therefore, the boundary Σ may be altered, leading to non-smooth jumps of the power flow solution.

In the case where the loads at certain buses can not be changed, the method presented can still be used. However, the load shedding will no longer be optimal.

Table 6.4: Testing results on optimal load shedding (162-bus system)

Iteration Number	$\|S^i - f(x^{i*})\|_2$	Min Eigvl	$\|S^0 - f(x^{i*})\|_2$
1	3.276	$4.255*10^{-5}$	3.276
2	1.509	$8.341*10^{-5}$	1.680
3	0.492	$-1.808*10^{-5}$	0.990
4	0.133	$1.209*10^{-7}$	0.907
5	0.050	$-5.368*10^{-3}$	0.906
6	0.229	$-5.800*10^{-5}$	0.988
7	0.089	$-3.858*10^{-4}$	0.964
8	0.029	$-1.970*10^{-3}$	0.963
9	0.076	$2.703*10^{-4}$	0.978
10	0.028	$-1.412*10^{-4}$	0.976
11	0.002		0.974

CHAPTER 7. CONCLUSION

In this research, we have introduced several important features to the existing continuation power flow. Simulation results on two standard testing systems, the New England 30-bus system and the 162-bus Iowa reduced system, have demonstrated their effectiveness. These new features include the following.

First, an optimal step length strategy has been derived and incorporated into the continuation power flow. The optimal step length is selected based on the sensitivity of bus reactive power generation to load change, this leads to the minimum number of steps in continuation power flow. Simulation results have verified these properties and also demonstrated a reduction in the number of Newton-Raphson iterations.

Second, the MW distance to the critical point and the MVAr reactive power reserve have proved to be an effective measure of margins to voltage instability. When compared to two other indices, the MW distance and reactive power reserve are much more sensitive over a much larger range of the load. Besides, the MW distance has a linear relationship to the total active power load. This property can be used to predict the final collapse even from the base case operating point (according to the load change direction and generation sharing scenario). Furthermore, our margins can be readily calculated with very little computation. Simulation results have demonstrated the superior performance of MW distance and MVAr reserve.

Third, the iterative procedure presented in Chapter 5 enables the continuation power flow to find the worst case load change scenario and the worst case margin to voltage instability. This is especially useful when there is no reliable load change forecast available. The worst case margin guarantees static voltage stability as long as the total active power load increase is not more than the margin, no matter what the load increase pattern is. The worst case load change scenario provides very useful information to power system operators for precautionary measures. Simulation results demonstrate that the proposed procedure is very effective when the critical boundary is convex.

Finally, with the introduction of the damped Newton-Raphson method with guaranteed convergence, the continuation power flow is able to deal with nonconvergent loads. By an iterative procedure, it is able to find an optimal load shedding that brings the load to the solvable region. This feature will be very useful in contingency analysis and power system planning. Simulation results demonstrated that our modifications have led to far superior performance compared with that of a similar algorithm in the literature, and if the unsolvable load is not too far from the critical boundary, then the iteration converges fairly quickly.

Future work in this direction will include the following aspects:

- The critical boundary in general may be not convex, that is one of the reasons why we could not get the result for 162-bus system. Future work should be concentrated on this particular aspect.
- Unsolvable power flow solution can be due to several reasons. In this thesis the case where large increase in load is considered to get unsolvable solution. However other cases where some type of outages that lead to unsolvable solution can be investigated.

BIBLIOGRAPHY

[1] North American Electric Reliability Council (NERC). *Survey of the Voltage Collapse Phenomenon.* Summary of the Interconnecting Dynamics task force's survey on the voltage collapse phenomenon, Aug. 1991.

[2] IEEE Working Group. "Voltage Stability of Power Systems: Concepts, Analytical tools, and Industry Experience." IEEE 90 TH 0358-2-PWR.

[3] Christy, C. D. *Analysis of Steady State Voltage Stability in Large Scale Power Systems.* M.S. Thesis, Iowa State University, Ames, IA, 1990.

[4] Rheiboldt, W. C. "Solution Fields of Nolinear Equations and Continuation Methods." *SIAM J. Num. Anal.*, vol. 19, pp. 653-669,1989.

[5] Flatabø, N., O. B. Fosso, R. Ognedal, T. Carlsen and K. R. Heggland. "A Method for Calculation of Margins to Voltage Instability Applied on the Norwegian System for Maintaining Required Security Level." 92 SM 395-5 PWRS, IEEE PES Summer Meeting, Seattle, WA, May 1992.

[6] Battula, S. *Sensitivity Based Continuation Power Flow.* M.S. Thesis, Iowa State University, Ames, IA, 1993.

[7] Rheinboldt, W. C. Numerical Analysis of Parameterized Nonlinear Equations. New York: John Wiley & Sons, 1968.

[8] Schlueter, R. A., A. G. Costi, J. E. Sekerke, and H. L. Forgey., Voltage Stability and Security Assessment. EPRI Publication, EL-5967, Aug. 1988.

[9] Zeng, Z. C., F. D. Galiana, B. T. Ooi and N. Yorino. "A Simple Approach to Estimate Maximum Loading Conditions in the Load Flow Problem." 92 WM-307-9 PWRS, IEEE PES Winter Meeting, New York, Jan. 1992.

[10] Galiana, F. D. and Z. C. Zeng. "Analysis of the Load Flow Behavior Near a Jacobian singularity." Proceedings of the IEEE Power Industry Computer Applications Conference, May 1991, pp. 149-155.

[11] Ajjarapu, V., and C. Christy. "The Continuation Power Flow: A Tool for Steady-State Voltage Stability Analysis." *IEEE Transactions on Power Systems*, vol. PWRS-7, pp. 416-423, Feb. 1992.

[12] Löf, P-A., G. Anderson, and D. J. Hill. "Voltage Stability Indices for Stressed Power System." 92 MW 101-6 PWRS, IEEE PES Winter Meeting, New York, Jan. 1992.

[13] Tiranuchit, A., and H. Glavistch. "Estimating the Voltage Stability of a Power System." *IEEE Transactions on Power Delivery*, vol. PWRD-1, pp. 346-354, July 1986.

[14] Ilic, M. and A. Stankovic. "Voltage Problems on Transmission Networks Subject to Unusual Power Flow Patterns." 88 WM 158-7 PWRS, IEEE PES Winter Meeting, New York, Jan. 1988.

[15] Dobson, I. and L. Lu, "New Methods for Computing a Closest Saddle Node Bifurcation and Worst Case Load Power Flow Margin for Voltage Collapse." 92 SM 395-5 PWRS, IEEE PES Summer Meeting, Seattle, WA, May 1992.

[16] Alvarado, F., I. Dobson, and Y. Hu. "Computation of Closest Bifurcation in Power Systems." 93 SM 484-6 PWRS, IEEE PES Summer Meeting, Vancouver, B. C., Canada, July, 1993.

[17] Dobson, I., L. Lu and Y. Hu. "A Direct Method for Computing a Closest Saddle Node Bifurcation in the Load Power Parameter Space of an Electric Power System." *IEEE ISCAS*, Singapore, June 1991, pp. 3019-3022.

[18] Dobson, I. and L. Lu, "Voltage Collapse Precipitated by Immediate Change in Stability When Generator Reactive Power Limits are Encountered." *IEEE Transactions on Circuits and System*, vol. 39, No. 9, September 1992.

[19] Fink, L. H. ed., "Bulk Power System Voltage Phenomena Voltage stability and Security." EPRI Report EL-6183, Potosi, Missouri, Jan. 1989.

[20] Iwamoto, S. and Y. Tamura. "A Load Flow Calculation Method for Ill-Conditioned Power Systems." *IEEE Trans. Power App. and Sys.*, vol. PAS-100, pp. 1736-1743, April 1981.

[21] Dehnel, M. and H. W. Dommel. "A Method for Identifying Weak Nodes in Nonconvergent Load flows." 88 SM 727-0, IEEE PES Summer Meeting, Portland, Oregon, May, 1988.

[22] Overbye, T. J. "A Power Flow Measure for Unsolvable Cases." 93 SM 484-6 PWRS, IEEE PES Summer Meeting, Vancouver, B. C., Canada, July, 1993.

APPENDIX A. ESTIMATE OF THE CRITICAL POINT

A.1 Introduction

In order for the continuation power flow to be used in real time in utilities, improving computational speed is a very important aspect. Since the amount of computation is proportional to the number of points we calculate on the solution path before the critical point is reached, it has been our objective to reduce the number of steps that is required by the use of optimal step lengths or maximum step lengths. The consequence of using maximum step lengths is reduced resolution of the traced solution path. As a result, we will in general be unable to find the exact solution of the critical point. The goal of this chapter is to provide a more accurate estimation of the critical point based on the available information from the continuation power flow. This improved estimation is obtained by solving a scalar nonlinear equation using Newton-Raphson algorithm plus some other scalar manipulations. Therefore, the computation needed for the improvement is minimal compared to that needed for solving the power flow equations, especially for large power systems.

The methodology presented in this chapter is based on the work done by the authors in [9-10]. we will provide a simplified derivation of the sensitivity of bus voltages to load changes near the critical point. In Section A.3, we generalize the estimation formu-

lae for the sensitivity coefficients and for the critical load change parameter such that they can be readily used in the continuation power flow. In Section A.4, we present an algorithm based on Newton's method to solve for the desired critical load parameter. Finally in Section A.5, we will present simulation results on the New England 30-bus test system.

A.2 Voltage Sensitivity near a Singular Point

Let z denote the vector of specified load flow injections and x denote the vector of bus voltage components in the Cartesian coordinates. Then, the power flow equation ofod choiceork is given by:

$$z = F(x)$$

In the Cartesian (rectangular) coordinates, the nonlinear function $F(x)$ is a second order function. Small changes dz, dx of z and x respectively will satisfy the following equation [9] :

$$dz = L(x_0)dx + Q(dx) \tag{A.1}$$

where

x_0: the operating point,

$$L(x_0) = \left.\frac{\partial F}{\partial x}\right|_{x=x_0}$$

$$dx = x - x_0$$

$$dz = z - F(x_0)$$

$$Q(dx) = \frac{1}{2}L(dx)dx$$

Since $F(x)$ is second order function in x, $L(x)$ is linear in x. To obtain the voltage sensitivity near a singular point, let us take $x_0 = x_s$= singular point. Then $L(x_s)$ is singular

with rank = $n-1$. Therefore, there exist column vectors v_1 and α such that

$$\begin{aligned} L(x_s)v_1 &= 0 \\ \alpha^T L(x_s) &= 0 \end{aligned} \tag{A.2}$$

Let $\{w_1, w_2, \cdots, w_{n-1}\}$ be the basis of the orthogonal complement of $span\{v_1\}$ and let $W = [w_1, w_2, \cdots, w_{n-1}]$. Then any vector can be expressed as a linear combination of v_1 and $w_k's$. Therefore, dx can be written in the form [10] :

$$dx = v_1 d\sigma + W d\mu \tag{A.3}$$

where $d\sigma$ is a scalar and $d\mu$ is an $n-1$ dimensional column vector. Substituting equations (A.2) and (A.3) into equation (A.1), we get

$$\begin{aligned} dz &= L(x_s)(v_1 d\sigma + W d\mu) + \frac{1}{2} L(v_1 d\sigma + W d\mu)(v_1 d\sigma + W d\mu) \\ &= L(x_s) W d\mu + \frac{1}{2} L(v_1) v_1 d\sigma^2 + \frac{1}{2} L(v_1) W d\mu d\sigma \\ &\quad + \frac{1}{2} L(W d\mu) v_1 d\sigma + \frac{1}{2} L(W d\mu) W d\mu \\ &= L(x_s) W d\mu + \frac{1}{2} L(v_1) v_1 d\sigma^2 + L(W d\mu) v_1 d\sigma + \frac{1}{2} L(W d\mu) W d\mu \end{aligned} \tag{A.4}$$

To solve for $d\sigma$ and $d\mu$ from the above equation, let us keep the lowest order terms and ignore higher order terms. Apparently when $|dz|$ is small, $|d\mu|$ will be roughly proportional to $|dz|$, and $|d\sigma|$ will be roughly proportional to $\sqrt{|dz|}$, rending the last two terms in higher order of dz. This is verified by the following calculation. Ignoring the last two terms in Equation (A.4), we get

$$dz = L(x_s) W d\mu + \frac{1}{2} L(v_1) v_1 d\sigma^2 \tag{A.5}$$

Pre-multiplying by α^T yields:

$$\alpha^T dz = \frac{1}{2} \alpha^T L(v_1) v_1 d\sigma^2$$

since $\alpha^T L(x_s) = 0$. This leads to the solution:

$$d\sigma = \sqrt{2\alpha^T dz \Big/ \alpha^T L(v_1)v_1} \tag{A.6}$$

Substituting back into equation (A.5) leads to

$$L(x_s)Wd\mu = dz - \frac{L(v_1)v_1}{\alpha^T L(v_1)v_1}\alpha^T dz$$

Since W spans the orthogonal complement of the null space of $L(x_s)$, $W^T L^T(x_s)L(x_s)W$ is nonsingular. Hence, we have

$$W^T L^T(x_s)L(x_s)Wd\mu = W^T L^T(x_s)\left(dz - \frac{L(v_1)v_1}{\alpha^T L(v_1)v_1}\alpha^T dz\right)$$

$$d\mu = \left(W^T L^T(x_s)L(x_s)W\right)^{-1} W^T L^T(x_s)(dz - \frac{L(v_1)v_1}{\alpha^T L(v_1)v_1}\alpha^T dz) \tag{A.7}$$

Equations (A.6) and (A.7) verify that $|d\sigma|$ and $|d\mu|$ are indeed proportional to $\sqrt{|dz|}$ and dz respectively.

In continuation power flow, we usually consider load changes of the form

$$z = z_0 + \lambda C$$

where z_0 is the vector of initial load, C is the vector of load change direction, and λ is the load change parameter. Then, the load at the critical point or the singular point is of the form:

$$z_s = z_0 + \lambda_s C$$

where λ_s is the load change parameter corresponding to the critical point. Then we have:

$$dz = z_s - z = (\lambda_s - \lambda)C$$

Substituting this into Equations (A.6) and (A.7) leads to

$$\begin{aligned} d\sigma &= \sqrt{\left|\frac{2\alpha^T C}{\alpha^T L(v_1)v_1}\right|} \cdot \sqrt{|\lambda_s - \lambda|} \\ &= k_1\sqrt{|\lambda_s - \lambda|} \end{aligned} \tag{A.8}$$

and $$d\mu = k_2(\lambda_s - \lambda) \tag{A.9}$$

where k_1 is a scalar and k_2 is an $n-1$ dimensional constant column vector. Using Equations (A.8) and (A.9), Equation (A.3) becomes

$$dx = v\sqrt{|\lambda_s - \lambda|} + \omega(\lambda_s - \lambda) \tag{A.10}$$

where

$$v = v_1 k_1$$

$$\omega = W k_2$$

are n dimensional constant column vectors, and

$$dx = x - x_s$$

with x and x_s being the corresponding power flow solution for z and z_s respectively. Although we started the derivation in the Cartesian space for simplicity, the qualitative relationship between dx and $\lambda_s - \lambda$ in Equation (A.10) holds for any coordinate system. Therefore, Equation (A.10) can be directly used in the continuation power flow.

A.3 Solution of v and ω in the Continuation Power Flow

From equation (A.10) we can see:

$$x_s = x - v\sqrt{|\lambda_s - \lambda|} - \omega(\lambda_s - \lambda)$$

Once v and ω are known, then x_s, the critical point, can be calculated using the above equation with x being the solution of any nearby point. Therefore, the focus is now being placed on the calculation of v and ω.

Suppose we have calculated many points on the power flow curve by using the continuation power flow method. Let x_1, x_2, x_3, x_4, x_5 be the five points closest to the critical point, and λ_1, λ_2, λ_3, λ_4, λ_5 be the corresponding load change parameters. Then

we have the following five equations obtained by applying Equation (A.10) to each of the five closest points:

$$-x_s + x_1 = v\sqrt{|\lambda_s - \lambda_1|} + \omega(\lambda_s - \lambda_1) \tag{A.11}$$

$$-x_s + x_2 = v\sqrt{|\lambda_s - \lambda_2|} + \omega(\lambda_s - \lambda_2) \tag{A.12}$$

$$-x_s + x_3 = v\sqrt{|\lambda_s - \lambda_3|} + \omega(\lambda_s - \lambda_3) \tag{A.13}$$

$$-x_s + x_4 = v\sqrt{|\lambda_s - \lambda_4|} + \omega(\lambda_s - \lambda_4) \tag{A.14}$$

$$-x_s + x_5 = v\sqrt{|\lambda_s - \lambda_5|} + \omega(\lambda_s - \lambda_5) \tag{A.15}$$

Upon subtracting Equation (A.11) from Equation (A.12), we get:

$$x_2 - x_1 = v\left(\sqrt{|\lambda_s - \lambda_2|} - \sqrt{|\lambda_s - \lambda_1|}\right) - \omega(\lambda_2 - \lambda_1)$$

Dividing this Equation by $\lambda_2 - \lambda_1$ leads to:

$$\Delta_1 = \frac{x_2 - x_1}{\lambda_2 - \lambda_1} = v\frac{\sqrt{|\lambda_s - \lambda_2|} - \sqrt{|\lambda_s - \lambda_1|}}{\lambda_2 - \lambda_1} - \omega \tag{A.16}$$

Similarly we can obtain three more equations of this form by using Equations (A.12) - (A.15):

$$\Delta_2 = \frac{x_3 - x_2}{\lambda_3 - \lambda_2} = v\frac{\sqrt{|\lambda_s - \lambda_3|} - \sqrt{|\lambda_s - \lambda_2|}}{\lambda_3 - \lambda_2} - \omega \tag{A.17}$$

$$\Delta_3 = \frac{x_4 - x_3}{\lambda_4 - \lambda_3} = v\frac{\sqrt{|\lambda_s - \lambda_4|} - \sqrt{|\lambda_s - \lambda_3|}}{\lambda_4 - \lambda_3} - \omega \tag{A.18}$$

$$\Delta_4 = \frac{x_5 - x_4}{\lambda_5 - \lambda_4} = v\frac{\sqrt{|\lambda_s - \lambda_5|} - \sqrt{|\lambda_s - \lambda_4|}}{\lambda_5 - \lambda_4} - \omega \tag{A.19}$$

Subtracting Equation (A.16) from Equation (A.17) results in:

$$\Delta\Delta_1 = \Delta_2 - \Delta_1 = v\left(\frac{\sqrt{|\lambda_s - \lambda_3|} - \sqrt{|\lambda_s - \lambda_2|}}{\lambda_3 - \lambda_2} - \frac{\sqrt{|\lambda_s - \lambda_2|} - \sqrt{|\lambda_s - \lambda_1|}}{\lambda_2 - \lambda_1}\right) \tag{A.20}$$

Similarly we can get from Equations (A.17) - (A.19)

$$\Delta\Delta_2 = \Delta_3 - \Delta_2 = v\left(\frac{\sqrt{|\lambda_s - \lambda_4|} - \sqrt{|\lambda_s - \lambda_3|}}{\lambda_4 - \lambda_3} - \frac{\sqrt{|\lambda_s - \lambda_3|} - \sqrt{|\lambda_s - \lambda_2|}}{\lambda_3 - \lambda_2}\right) \quad \text{(A.21)}$$

and

$$\Delta\Delta_3 = \Delta_4 - \Delta_3 = v\left(\frac{\sqrt{|\lambda_s - \lambda_5|} - \sqrt{|\lambda_s - \lambda_4|}}{\lambda_5 - \lambda_4} - \frac{\sqrt{|\lambda_s - \lambda_4|} - \sqrt{|\lambda_s - \lambda_3|}}{\lambda_4 - \lambda_3}\right) \quad \text{(A.22)}$$

Substituting Equation (A.20) from Equation (A.21), yields:

$$\Delta\Delta\Delta_1 = v\left(\frac{\sqrt{|\lambda_s - \lambda_4|} - \sqrt{|\lambda_s - \lambda_3|}}{\lambda_4 - \lambda_3} - 2\frac{\sqrt{|\lambda_s - \lambda_3|} - \sqrt{|\lambda_s - \lambda_2|}}{\lambda_3 - \lambda_2} + \frac{\sqrt{|\lambda_s - \lambda_2|} - \sqrt{|\lambda_s - \lambda_1|}}{\lambda_2 - \lambda_1}\right) \quad \text{(A.23)}$$

Substituting Equation (A.21) from Equation (A.22), yields:

$$\Delta\Delta\Delta_2 = v\left(\frac{\sqrt{|\lambda_s - \lambda_5|} - \sqrt{|\lambda_s - \lambda_4|}}{\lambda_5 - \lambda_4} - 2\frac{\sqrt{|\lambda_s - \lambda_4|} - \sqrt{|\lambda_s - \lambda_3|}}{\lambda_4 - \lambda_3} + \frac{\sqrt{|\lambda_s - \lambda_3|} - \sqrt{|\lambda_s - \lambda_2|}}{\lambda_3 - \lambda_2}\right) \quad \text{(A.24)}$$

Finally let us define: $\Delta t = \dfrac{\|\Delta\Delta\Delta_2\|}{\|\Delta\Delta\Delta_1\|}$, then we have

$$\Delta t = \frac{\left\|\dfrac{\sqrt{|\lambda_s - \lambda_5|} - \sqrt{|\lambda_s - \lambda_4|}}{\lambda_5 - \lambda_4} - 2\dfrac{\sqrt{|\lambda_s - \lambda_4|} - \sqrt{|\lambda_s - \lambda_3|}}{\lambda_4 - \lambda_3} + \dfrac{\sqrt{|\lambda_s - \lambda_3|} - \sqrt{|\lambda_s - \lambda_2|}}{\lambda_3 - \lambda_2}\right\|}{\left\|\dfrac{\sqrt{|\lambda_s - \lambda_4|} - \sqrt{|\lambda_s - \lambda_3|}}{\lambda_4 - \lambda_3} - 2\dfrac{\sqrt{|\lambda_s - \lambda_3|} - \sqrt{|\lambda_s - \lambda_2|}}{\lambda_3 - \lambda_2} + \dfrac{\sqrt{|\lambda_s - \lambda_2|} - \sqrt{|\lambda_s - \lambda_1|}}{\lambda_2 - \lambda_1}\right\|}$$

$$= \pm \frac{\frac{\sqrt{|\lambda_s - \lambda_5|} - \sqrt{|\lambda_s - \lambda_4|}}{\lambda_5 - \lambda_4} - 2\frac{\sqrt{|\lambda_s - \lambda_4|} - \sqrt{|\lambda_s - \lambda_3|}}{\lambda_4 - \lambda_3} + \frac{\sqrt{|\lambda_s - \lambda_3|} - \sqrt{|\lambda_s - \lambda_2|}}{\lambda_3 - \lambda_2}}{\frac{\sqrt{|\lambda_s - \lambda_4|} - \sqrt{|\lambda_s - \lambda_3|}}{\lambda_4 - \lambda_3} - 2\frac{\sqrt{|\lambda_s - \lambda_3|} - \sqrt{|\lambda_s - \lambda_2|}}{\lambda_3 - \lambda_2} + \frac{\sqrt{|\lambda_s - \lambda_2|} - \sqrt{|\lambda_s - \lambda_1|}}{\lambda_2 - \lambda_1}}$$

Since by definition Δt is always positive, the "+" sign should be used if the value of the fraction is positive and "-" sign should be used if otherwise. Define $f(\lambda_s)$ by

$$f(\lambda_s) = \frac{\sqrt{|\lambda_s - \lambda_5|} - \sqrt{|\lambda_s - \lambda_4|}}{\lambda_5 - \lambda_4} - 2\frac{\sqrt{|\lambda_s - \lambda_4|} - \sqrt{|\lambda_s - \lambda_3|}}{\lambda_4 - \lambda_3} + \frac{\sqrt{|\lambda_s - \lambda_3|} - \sqrt{|\lambda_s - \lambda_2|}}{\lambda_3 - \lambda_2}$$

$$\mp \Delta t \cdot \left(\frac{\sqrt{|\lambda_s - \lambda_4|} - \sqrt{|\lambda_s - \lambda_3|}}{\lambda_4 - \lambda_3} - 2\frac{\sqrt{|\lambda_s - \lambda_3|} - \sqrt{|\lambda_s - \lambda_2|}}{\lambda_3 - \lambda_2} + \frac{\sqrt{|\lambda_s - \lambda_2|} - \sqrt{|\lambda_s - \lambda_1|}}{\lambda_2 - \lambda_1} \right)$$

Then λ_s satisfies the equation:

$$f(\lambda_s) = 0 \tag{A.25}$$

Notice that from their definitions, $\Delta_1, \cdots \Delta_4$, $\Delta\Delta_1, \cdots \Delta\Delta_3$, $\Delta\Delta\Delta_1$, $\Delta\Delta\Delta_2$ and Δt are calculated from $x_1, \cdots x_5$ and $\lambda_1, \cdots \lambda_5$ only. Therefore, they are readily available once we have calculated five points in the continuation power flow.

The solution of Equation (A.25) will be discussed in the next section. Once λ_s is solved, Equation (A.24) can be used to solve for v as

$$v = \frac{\Delta\Delta\Delta_2}{\frac{\sqrt{|\lambda_s - \lambda_5|} - \sqrt{|\lambda_s - \lambda_4|}}{\lambda_5 - \lambda_4} - 2\frac{\sqrt{|\lambda_s - \lambda_4|} - \sqrt{|\lambda_s - \lambda_3|}}{\lambda_4 - \lambda_3} + \frac{\sqrt{|\lambda_s - \lambda_3|} - \sqrt{|\lambda_s - \lambda_2|}}{\lambda_3 - \lambda_2}} \tag{A.26}$$

With this solution, equation (A.19) can be rewritten as

$$\omega = v\frac{\sqrt{|\lambda_s - \lambda_5|} - \sqrt{|\lambda_s - \lambda_4|}}{\lambda_5 - \lambda_4} - \Delta_4 \tag{A.27}$$

that gives the solution for ω. Once we have v and ω, we can use Equation (A.15) to calculate the critical point $x_s$as follows:

$$x_s = x_5 - v\sqrt{\lambda_s - \lambda_5} - \omega(\lambda_s - \lambda_5) \qquad \text{(A.28)}$$

Note that we have used Equations (A.24), (A.19) and (A.15) to calculated v, ω, x_s respectively. We could have used any other combination, such as Equations (A.20), (A.16) and (A.11), for the same purpose. The reason of our choice is as follows. The five points x_1, x_2, x_3, x_4, x_5 from the continuation power flow are of different distances to the critical point. The last point, i. e. x_5 is closet to the critical point, hence we use Equations (A.23), (A.19) and (A.15) instead of any others. Therefore, our numerical error is the smallest.

A.4 Solution of the Critical Load Change Parameter λ_s

From the discussion of last section, once λ_s is calculated, Equations (A.26) and (A.27) can be easily used to obtain v and ω respectively, then the Equations (A.28) gives the vector of bus voltages at the critical load. Therefore, the key is to solve λ_s. Recall from last section that λ_s has to satisfy

$$f(\lambda_s) = 0 \qquad \text{(A.25)}$$

which is a nonlinear equation. Newton's method can be used to solve Equation (A.25). To derive the formula, let λ_0 be an initial guess for λ_s (the selection of λ_0 will be discussed later). Then the first order Taylor series approximation of $f(\lambda_s)$ leads to

$$f(\lambda_0) + \left.\frac{df}{d\lambda}\right|_{\lambda=\lambda_s} (\lambda_s - \lambda_0) = 0$$

Solving for λ_s yields

$$\lambda_s = \lambda_0 - f(\lambda_0) \Big/ \left.\frac{df}{d\lambda}\right|_{\lambda=\lambda_0}$$

Writing in a recursive form, the above equation becomes:

$$\lambda_{k+1} = \lambda_k - f(\lambda_k) \Big/ \left.\frac{df}{d\lambda}\right|_{\lambda=\lambda_k} \tag{A.29}$$

By the definition of $f(\lambda_s)$, we have

$$f(\lambda_k) = \frac{\sqrt{|\lambda_k - \lambda_5|} - \sqrt{|\lambda_k - \lambda_4|}}{\lambda_5 - \lambda_4} - 2\frac{\sqrt{|\lambda_k - \lambda_4|} - \sqrt{|\lambda_k - \lambda_3|}}{\lambda_4 - \lambda_3} + \frac{\sqrt{|\lambda_k - \lambda_3|} - \sqrt{|\lambda_k - \lambda_2|}}{\lambda_3 - \lambda_2}$$

$$\mp\Delta t\left(\frac{\sqrt{|\lambda_k - \lambda_4|} - \sqrt{|\lambda_k - \lambda_3|}}{\lambda_4 - \lambda_3} - 2\frac{\sqrt{|\lambda_k - \lambda_3|} - \sqrt{|\lambda_k - \lambda_2|}}{\lambda_3 - \lambda_2} + \frac{\sqrt{|\lambda_k - \lambda_2|} - \sqrt{|\lambda_k - \lambda_1|}}{\lambda_2 - \lambda_1}\right) \tag{A.30}$$

$$\left.\frac{df}{d\lambda}\right|_{\lambda=\lambda_k} = \frac{\frac{1}{\sqrt{\lambda_k - \lambda_5}} - \frac{1}{\sqrt{\lambda_k - \lambda_4}}}{2(\lambda_5 - \lambda_4)} + (\mp\frac{\Delta t}{2} - 1)\frac{\frac{1}{\sqrt{\lambda_k - \lambda_4}} - \frac{1}{\sqrt{\lambda_k - \lambda_3}}}{(\lambda_4 - \lambda_3)}$$

$$+(1 \pm \frac{\Delta t}{2})\frac{\frac{1}{\sqrt{\lambda_k - \lambda_3}} - \frac{1}{\sqrt{\lambda_k - \lambda_2}}}{(\lambda_3 - \lambda_2)} \mp \Delta t\frac{\frac{1}{\sqrt{\lambda_k - \lambda_2}} - \frac{1}{\sqrt{\lambda_k - \lambda_1}}}{2(\lambda_2 - \lambda_1)} \tag{A.31}$$

Then the recursive computer algorithm for calculating λ_s looks like this:

1) Select ε, λ_0, set $k = 1$
2) Calculate f_k using Equation (A.30)
3) Calculate $\frac{df_k}{d\lambda}$ using Equation (A.31)
4) If $\left| f_k \Big/ \frac{df_k}{d\lambda} \right| < \varepsilon$, stop

5) Set $\lambda_k = \lambda_{k-1} - f_k \Big/ \frac{df_k}{d\lambda}$

6) Set $k = k+1$, go to 2)

This seemingly simple algorithm will not work well if brutally implemented. The difficulty comes from the specific form of the function $f(\lambda_s)$, which is not friendly at all to the Newton algorithm. Figure A.1 illustrates one typical shape of the function. First, if, during iteration, λ_k happens to be exactly one of those five points (λ_1, λ_2, λ_3, λ_4, λ_5) from continuation power flow , then $f_k \Big/ \frac{df_k}{d\lambda} = 0$, and λ_k will not be updated any more.

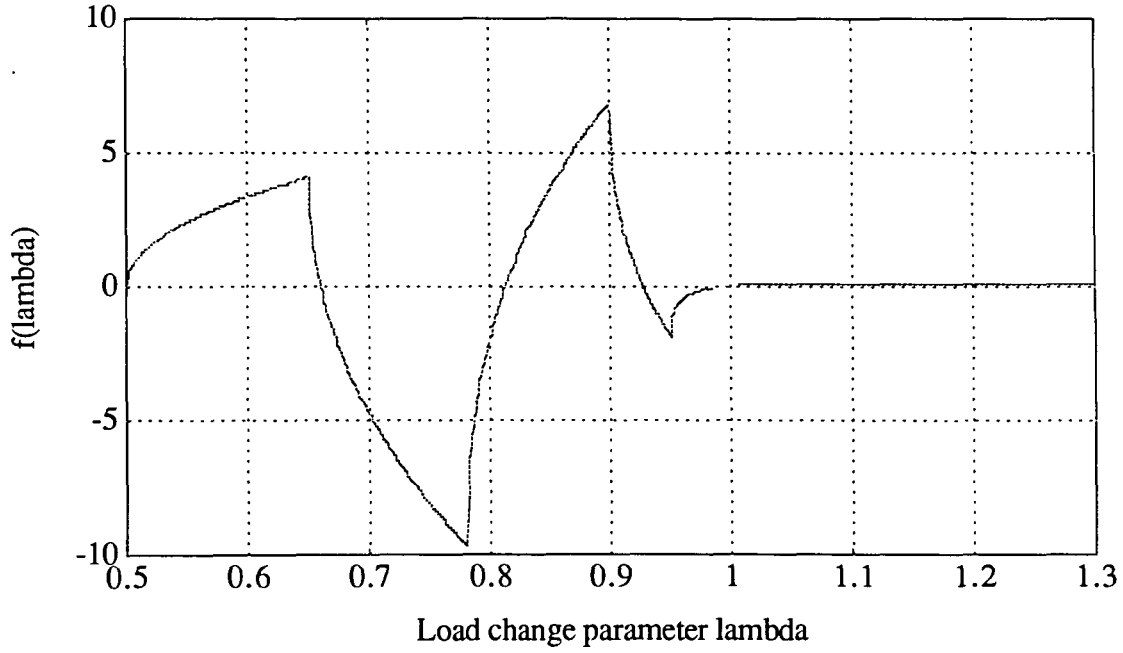

Figure A.1: A Typical curve of $f(\lambda)$ vs λ

This gives a false convergence, since $\lambda_k \neq \lambda_s$. Second, if λ_k is not exactly but very close to one of those five points, then $\frac{df_k}{d\lambda}$ may be exceedingly large and cause numerical problem, since $f(\lambda_k)$ is not differentiable at those five points. Finally, some segments of the curve $f(\lambda)$ are quite flat, therefore $\frac{df_k}{d\lambda}$ may be very small, sending x_k far away from the true solution. Consequently, λ_k will oscillate between the two sides of λ_5 and may grow unbounded in magnitude. All these three situations have appeared in our simulation. To avoid these complications, two measures must be taken: proper selection of initial guess λ_0, and use of hard limit to bound λ_k. First the initial guess cannot be arbitrarily selected because of the above three mentioned difficulties. For the Newton's algorithm to work better, the initial guess λ_0 should be as close to λ_s as possible. Since the five points λ_1, λ_2, λ_3, λ_4, λ_5 are obtained using iterative method in the continuation power flow, it is always the case that λ_5 is closest to λ_s and λ_4 is the second closest. It is also always true that $\lambda_4 < \lambda_5$. But λ_5 is the last point from continuation power flow, it may be greater than λ_s or may be smaller. This can be indicated by the voltage stability index available from continuation power flow program. If the index is greater than zero, $\lambda_5 < \lambda_s$, if the index is negative, $\lambda_5 > \lambda_s$. In the case $\lambda_5 > \lambda_s$, a very good choice for λ_0 would be the mid-point between λ_4 and λ_5. In the case $\lambda_5 < \lambda_s$, we select λ_0 to be a little larger than λ_5. Since we know λ_5 is already quite close to λ_s, a 10% increase from λ_5 may be a good choice.

In summary the initial guess λ_0 are to be selected as follows:

$$\begin{cases} \text{if } index > 0, \quad \lambda_0 = 1.1\lambda_5 \\ \text{if } index < 0, \quad \lambda_0 = \dfrac{\lambda_4 + \lambda_5}{2} \end{cases}$$

This takes care of the selection of the initial guess. But during iteration, λ_k can also become unstable. To prevent this, we use an upper and a lower limit to bound λ_k. The selection of the limits are also dependent on the two cases: $\lambda_5 > \lambda_s$ and $\lambda_5 < \lambda_s$. If $\lambda_5 > \lambda_s$, we know λ_s must be between λ_4 and λ_5. Therefore, we select $\lambda_l = \lambda_4 + \varepsilon$, and $\lambda_u = \lambda_5 - \varepsilon$. If $\lambda_5 < \lambda_s$, then we select $\lambda_l = \lambda_5 + \varepsilon$, and $\lambda_u = 1.5\lambda_5$.

Incorporating these discussions to the Newton's algorithm, we have:

Newton's Algorithm for calculating λ_s:

1) Select $\varepsilon(=10^{-6})$, set $k=1$

2) if voltage stability index > 0

   set $\lambda_0 = 1.1\lambda_5$, $\lambda_l = \lambda_5 + \varepsilon$, $\lambda_u = 1.5\lambda_5$

   if voltage stability index < 0

   set $\lambda_0 = \dfrac{\lambda_4 + \lambda_5}{2}$, $\lambda_l = \lambda_4 + \varepsilon$, $\lambda_u = \lambda_5 - \varepsilon$

3) Calculate f_k using Equation (A.30)

4) Calculate $\dfrac{df_k}{d\lambda}$ using Equation (A.31)

5) If $\left| f_k \Big/ \dfrac{df_k}{d\lambda} \right| < \varepsilon$, go to 9)

6) Let $\lambda_k = \lambda_{k-1} - f_k \Big/ \dfrac{df_k}{d\lambda}$

7) If $\lambda_k < \lambda_l$, then $\lambda_k = \lambda_l$

   Else if $\lambda_k > \lambda_u$, then $\lambda_k = \lambda_u$

8) Set $k = k+1$

9) Stop

A.5 Simulation Results

The proposed scheme for estimating the critical point has tested on the New England 30-bus system. The regular continuation power flow method is first applied to find a sequence of points on the solution path assuming a standard load change scenario. The last five points are the closest to the critical point to be found. The corresponding load change parameters are :

$$\lambda_1=0.0969$$

$$\lambda_2=0.1240$$

$$\lambda_3=0.1281$$

$$\lambda_4=0.1337$$

$$\lambda_5=0.1342$$

using these five points a nonlinear function $f(\lambda_s)$ can be defined and the procedure from the last section is applied to find $\lambda_s=0.1400$.

To verify that $\lambda_s=0.1400$ is indeed very close to the critical point, we have also used the continuation power flow with very small step lengths to find the critical point. The critical load change parameter found this way is $\lambda_s=0.1346$. It is apparent that the two methods led to very similar solutions. Since, at the expense of large computation with small step length, the critical load change parameter from the continuation power flow is quite accurate. However, since the estimate uses scalar manipulation after a continuation power flow run with large step length, the computation involved is significantly smaller.

APPENDIX B. OPTIMAL MULTIPLIER METHOD [19]

The optimal multiplier method [19] transforms the problem of solving $F(x)=0$ to a minimization problem $\min_x G(x)=[F(x)]^T F(x)$ which is further reduced to a scalar problem $\min_\mu G(\mu)=G(x(\mu))=[F(x_k-\mu\Delta x_k)]^T F(x_k-\mu\Delta x_k)$ where $\Delta x_k = J^{-1}F(x_k)$ and μ is "optimal multiplier". To solve for the optimal multiplier μ the power flow equation is formulated in the Cartesian coordinates in the form:

$$F(x)=y_s-y(x)=0$$

where y_s is the set load and $y(x)$ is a second order hermitian function of x. Because of the hermitian property,

$$\begin{aligned} F(x_k-\mu\Delta x_k) &= y_s-y(x_k)+\mu J(y(x_k))\Delta x_k-\mu^2 y(\Delta x_k) \\ &= a+\mu b+\mu^2 c \end{aligned} \tag{B.1}$$

where $a=y_s-y(x_k)$

$b=J(y(x_k))\Delta x_k$

$c=-y(\Delta x_k)$

Substituting (B.1) into (6.6) we get

$$G(\mu)=(a+\mu b+\mu^2 c)^T(a+\mu b+\mu^2 c)$$

To solve for the minimizing μ we set

$$\frac{dG(\mu)}{d\mu}=2(a+\mu b+\mu^2 c)^T(b+2\mu c)=0$$

$$a^T b+(2a^T c+b^T b)\mu+3b^T c\mu^2+2c^T c\mu^3=0$$

The above equation is a third order scalar polynomial equation, therefore can be easily solved using cardan formula. In this method, the total mismatch $G(\mu)$ is guaranteed to decrease in each step. For solvable loads, $\mu^* \approx 1$. For unsolvable loads, $\mu^* \to 0$.